Technical Report

TR-03-03

Experimental determination and chemical modelling of radiolytic processes at the spent fuel/ water interface

Experiments carried out in carbonate solutions in absence and presence of chloride

Jordi Bruno, Esther Cera, Mireia Grivé, Lara Duro
Enviros Spain SL, Spain

Trygve Eriksen
Dept Nuclear Chemistry, KTH, Sweden

January 2003

Svensk Kärnbränslehantering AB
Swedish Nuclear Fuel
and Waste Management Co
Box 5864
SE-102 40 Stockholm Sweden
Tel 08-459 84 00
+46 8 459 84 00
Fax 08-661 57 19
+46 8 661 57 19

Experimental determination and chemical modelling of radiolytic processes at the spent fuel/ water interface

Experiments carried out in carbonate solutions in absence and presence of chloride

Jordi Bruno, Esther Cera, Mireia Grivé, Lara Duro
Enviros Spain SL, Spain

Trygve Eriksen
Dept Nuclear Chemistry, KTH, Sweden

January 2003

Keywords: radionuclides, radiolysis products, spent fuel, thermodynamic.

Abstract

We report on the recent experimental and modelling results of a research programme that started in 1995. The aim has been to understand the kinetic and thermodynamic processes that control the radiolytic generation of oxidants and reductants at the spent fuel water interface and their consequences for spent fuel matrix stability and radionuclide release. This has been done by carrying out well-controlled dissolution experiments of PWR Ringhals spent fuel fragments in an initially anoxic closed system and by using different solution compositions. Experimental series started with several tests carried out with deionised water as solvent /Eriksen et al, 1995/, in a second phase experiments were conducted with 10 mM bicarbonate solutions /Bruno et al, 1999/.

New experimental series were set up during the last two years by using the same bicarbonate content in solutions with varying NaCl concentrations in order to ascertain the role of this ligand on the radiolytic products and its consequence for radionuclide release. The selected NaCl concentrations are in the range of 0.1 to 10 mM.

Experimental data shows that uranium dissolution at early contact times is controlled by the oxidation of the UO_2 matrix. This process controls the co-dissolution of most of the analysed radionuclides, including Sr, Mo, Tc, Np and surprisingly enough, Cs. In the overall the release rates for U and the matrix associated radionuclides are in the range of 10^{-6} moles/day with a clear decreasing trend with exposure time and after 2 years the initial release rates have decreased down to $3\ 10^{-8}$ moles/day.

The solubility of the released actinides appears to be limited by the formation of An(IV) hydroxide phases, although Np concentrations in solution did not reach solubility levels during the time intervals of the present tests. No secondary solid phase appears to control the solubility of the rest of the elements.

Contents

1 Introduction

The chemical stability of a repository is defined by its resistance to radionuclide release to the biosphere. This resistance is primarily dependent on the chemical stability of the spent fuel matrix itself and the chemical conditions of its disposal. These chemical conditions are designed and engineered in order to minimise the potential release of radionuclides and are normally described by two intensive parameters (pH and Eh). It is clear that the redox potential is the most critical one to define the stability of the spent fuel matrix given the narrower variability expected in pH values besides the lower effect of pH on the solubility of UO_2. In this context, it is now well established that the confinement of radionuclides within the matrix is guaranteed if the oxidation state of the UO_2 matrix does not exceed the upper limit of stability of the cubic structure, $UO_{2.33}$, which corresponds to a nominal stoichiometry of U_3O_7 /Johnson and Shoesmith, 1988; Shoesmith, 2001/.

However, the spent fuel matrix constitutes a dynamic redox system by itself. This is because there is a time-dependent generation of oxidants and reductants at the fuel/water interface due to α, β and γ radiolysis. Under these circumstances, it is problematic to treat the spent fuel/water system as a redox equilibrium and consequently the definition of Eh (or pe) as an intensive parameter becomes questionable. The complexity is further increased when we try to integrate additional redox-sensitive components, like Cu and Fe from the canister or the pyrite content of the bentonite material, into the system under study.

The role of mineral surfaces in poising the redox state of a solid/water system is a well established phenomenon evolving from the concepts developed for heterogeneous electron transfer /White and Yee, 1985/. The fact that the UO_2 spent fuel matrix constitutes a semiconductor would indicate that the basic premises for heterogeneous electron transfer reactions are fulfilled. In the repository situation where the "Mass to Volume" ratio is particularly high, the UO_2 surface is going to play a key role in defining the redox capacities of the system and, consequently, its redox state.

Experimental evidence on the active redox role of the UO_2 surfaces is now available. /Eriksen et al, 1995/ and /Bruno et al, 1999/, reported on well controlled experiments aimed at obtaining the mass balance of radiolytically produced oxidants and reductants by spent fuel in contact with distilled water and carbonate solutions respectively. In these experiments, performed in a closed system, a clear oxidant deficit was observed. The authors explained this oxidant deficit by the effect of their uptake by the UO_2 spent fuel surface. Natural uraninite deposits have also brought clear indications of the redox buffering capacity of the UO_2 surface. Redox measurements performed in groundwaters in contact with the uraninite deposits in Cigar Lake (Canada) /Casas and Bruno, 1994/ and Palmottu (Finland) /Bruno et al, 1996; Cera et al, 2002/, indicate that the redox potential could be poised by the UO_2/U_3O_7 transition.

This work is the continuation of the experimental and modelling programme started in 1998 with the first four series of tests, the so-called time resolved tests, performed in 10 mM bicarbonate solutions /Bruno et al, 1999/. New series of experiments have been carried out by using the same bicarbonate content but with varying NaCl concentrations in order to ascertain the role of chloride on the radiolytic products and its consequence for radionuclide release.

The selected NaCl concentrations are in the range of 0.1 to 10 mM. This range of chloride concentrations is found in most of the Swedish granitic groundwaters.

The main objective of this report is to present the newly acquired experimental data which will be modelled together with the previously reported set of data in /Bruno et al, 1999/.

2 Experimental

2.1 Material

Fragments from a PWR fuel rod, Ringhals DO-7-S14 were used in the experiments. The Ringhals DO-7-S14 fuel rod was irradiated for five cycles during 1977–1983 with an average linear power of 18 kW/m. The average calculated burnup is 40 MWd/kgU. These fuel fragments were the same as the ones used in the first tests /Bruno et al, 1999/. The weight of the fragments used in each experiment was approximately 2 g. Test solutions were prepared from Millie-Q purified water purged with AGA 5.7 quality argon, containing less than 0.5 ppm oxygen. $NaHCO_3$ and NaCl PA quality were used.

2.2 Experimental set up

The experimental set up is depicted in Figure 1. Fuel fragments were transferred to a quartz vessel with a total volume of 60 cm^3 approximately. The vessel containing the fuel fragments was mounted in a lead shield, placed in a glove box with argon atmosphere and connected to gas and solution sampling and analysing systems.

The test dissolution vessel and sensor chamber were flushed with argon through a thin plastic tube inserted into the vessel via the sensor chamber. A volume of 30cm^3 solution was transferred through the same plastic tube to the vessel by applying argon overpressure to a stock solution reservoir. The tube was thereafter removed and the valve connecting the reaction vessel and sensor chamber closed.

We report on 21 replenishment experiments in this report. Test 7.40.1 to 7.40.4 have been already reported /Bruno et al, 1999/, however, they are also included in the present analysis for comparison. Gas and solution analyses were carried out at several time intervals in order to follow the evolution of H_2, O_2, and H_2O_2 production as well as the release of the major component of the matrix, uranium and of several radionuclides. The initial solution composition of each run as well as the starting and finishing dates are given in Table 1.

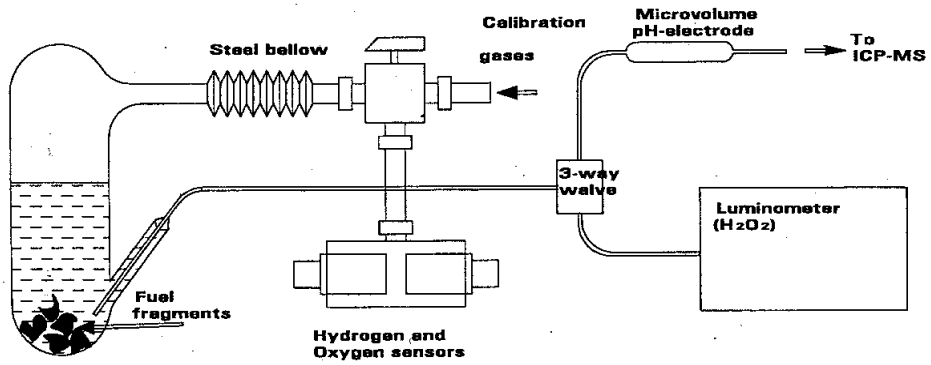

Figure 1. *Experimental set up.*

Table 1. Initial solution composition of each run.

	$NaHCO_3$ (mM)	NaCl (mM)		$NaHCO_3$ (mM)	NaCl (mM)
7.40.1	10		**7.40.11**	10	1
7.40.2	10		**7.40.12**	10	
7.40.3	10		**7.40.13**	10	1
7.40.4	10		**7.40.14**	10	1
7.40.5	10	0.1	**7.40.15**	10	0.1
7.40.6	10	0.1	**7.40.16**	10	0.1
7.40.7	10	1	**7.40.17**	10	0.1
7.40.8	10	1	**7.40.18**	10	0.1
7.40.9	10		**7.40.19**	10	10
7.40.10	10	0.1	**7.40.22**	10	
7.40.11	10	1	**7.40.23**	10	

2.3 Gas analysis

The oxygen and hydrogen gas detector system (Orbisphere 3600/111E, 31130 O_2 and 3600/2111E 31230 H_2 detectors) was calibrated by flushing the sensor chamber with standardised gas mixtures. After calibration the sensor chamber was flushed with argon, and the inlet and outlet valves closed. The reaction vessel/sensor chamber valve was thereafter opened allowing the radiolytically formed oxygen and hydrogen to diffuse into the sensor chamber. Detector readings were taken at time intervals to minimise oxygen and hydrogen consumption by the detectors.

2.4 Solution analysis

Small volumes (1–2 cm^3) of the test solution were removed through a capillary tube for analysis at given time intervals.

Hydrogen peroxide was measured by means of a luminescence method earlier described in detail by /Eriksen et al, 1995/.

Fission products were analysed with ICP-MS (Plasma Quad 2 Plus, VG Elemental UK). The analytical samples were prepared with a 1 ppb internal ^{115}In reference standard. Mass peak counts over the whole range (82 to 254) are related to the ^{115}In signal, yielding a series of ratios. Sensitivity factors relative to ^{115}In were determined using a range of natural multielement standards and radionuclide standards for Tc-99 and Pu. The uranium concentration was also measured using laser fluorimetry (Scintrex UA-3).

3 Results

3.1 Radiolysis products

The concentrations of the oxidants and reductants generated by the radiolysis of water as a function of the contact time are given in the following figures. Experiments are first grouped as a function of the initial chloride content in the test solution. At the end of this section, a comparison of the results obtained as a function of the chloride content is also presented.

3.1.1 Tests in the absence of NaCl

Eight runs were carried out by using a solution containing 10 mM of $NaHCO_3$. Figure 2 shows three plots of the hydrogen and oxygen concentrations in the gas phase and hydrogen peroxide concentrations respectively as a function of time.

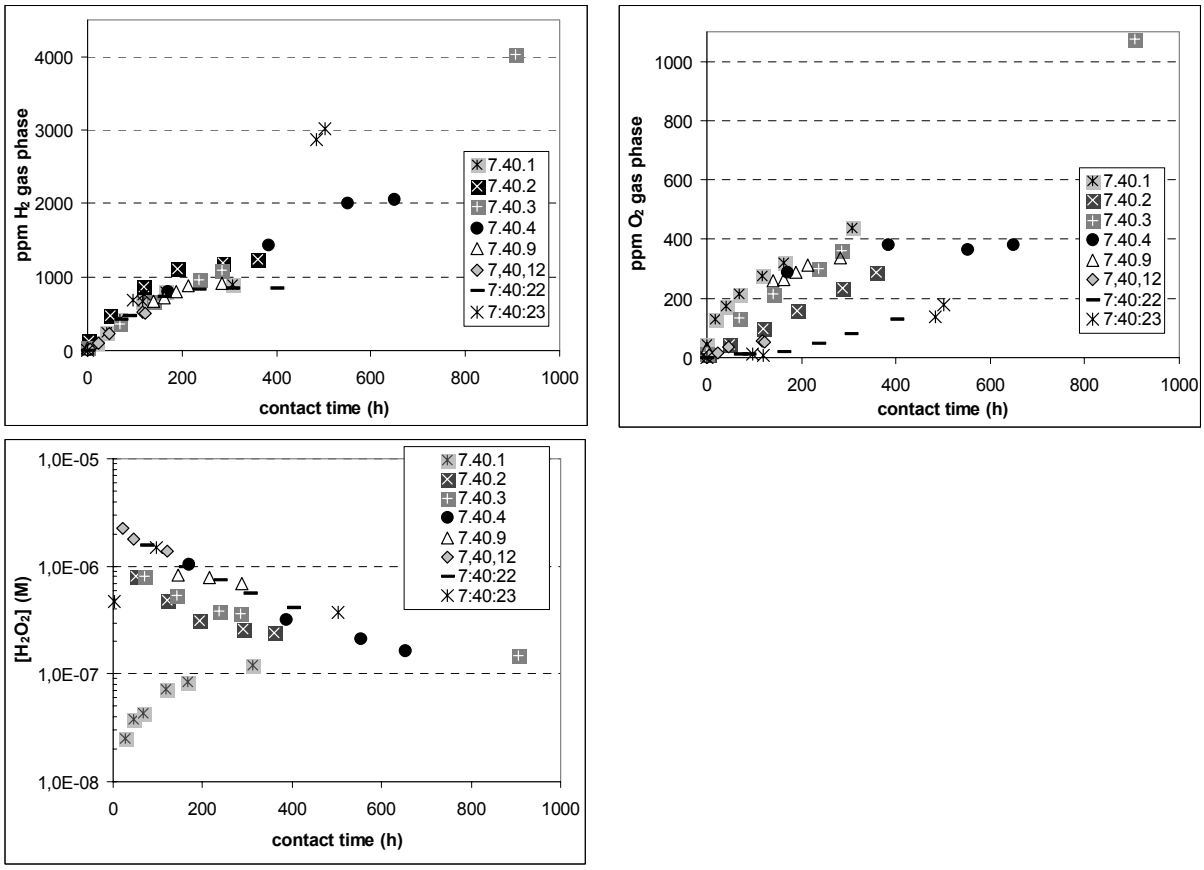

Figure 2. *Concentrations of hydrogen and oxygen in the gas phase and hydrogen peroxide in solution as a function of time. Data gathered at 10 mM $NaHCO_3$.*

As we can see in the first plot, hydrogen concentrations increase continuously with time. The evolution of the radiolytic products with time is quite similar as for the previously reported experiments /Bruno et al, 1999/. This is a proof of the reproducibility of the experiments. Oxygen concentrations follow the same trend as hydrogen, showing a continuous increase with time. A closer analysis of the data allows distinguishing between two different behaviours of oxygen in the system. There is a first set of experiments where maximum O_2 concentrations are on the order of 400 ppm and a second set where this maximum is of around 200 ppm. In general, hydrogen concentrations are larger than oxygen ones, as expected.

The evolution of hydrogen peroxide concentration with time also shows two different kinds of behaviour. In the first run, the concentration of hydrogen peroxide increases with time, while in the successive experiments, the concentration of hydrogen peroxide decreases with contact time until reaching a steady state. The net generation of hydrogen peroxide in all the runs is lower than the one of oxygen or hydrogen.

3.1.2 Experiments in 0.1 mM NaCl in solution

Seven runs were carried out by using a solution containing 10 mM $NaHCO_3$ and 0.1 mM NaCl. Figure 3 shows the evolution of hydrogen and oxygen concentrations in the gas phase and hydrogen peroxide concentrations in solution with time.

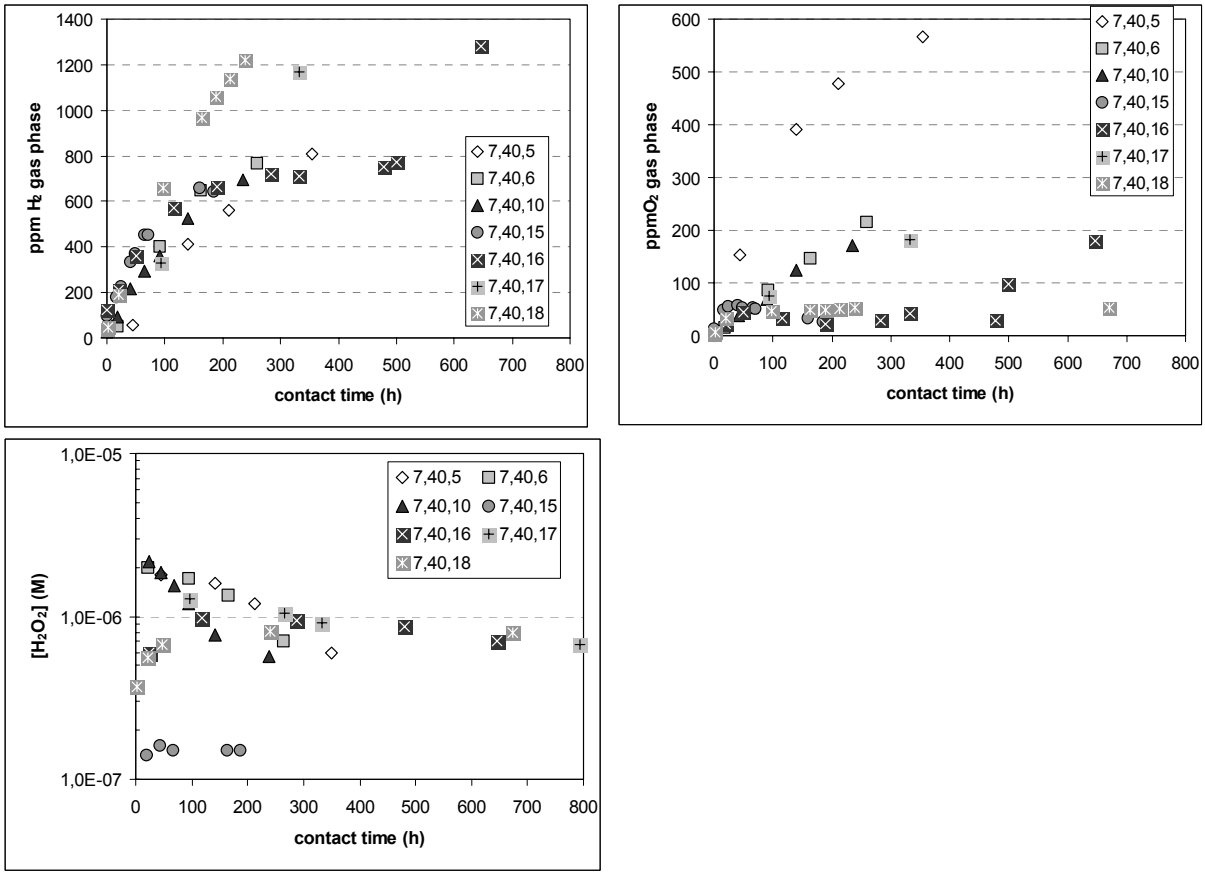

Figure 3. *Concentrations of hydrogen and oxygen in the gas phase and hydrogen peroxide in solution as a function of time. Data gathered at 10 mM $NaHCO_3$ and 0.1 mM NaCl.*

In this case we can also observe a continuous increase of the hydrogen concentration with time. The measured hydrogen concentrations are also comparable in most of the tests, although in one of the runs (7.40.16) hydrogen concentration larger than in the rest of the experiments are measured. Oxygen concentrations follow the same trend as hydrogen, since they also increase with time. However, as in the previous series, we can differentiate several slopes in the graph indicating different generation rates for this gas. The largest oxygen concentrations are obtained in test 7.40.5, reaching values quite close to the ones measured for hydrogen in the same experiment. Tests 7.40.6, 7.40.10 and 7.40.17 follow a different slope reaching concentrations around 200 ppm at the end of each run indicating a lower effective oxygen production with respect to the previous one. Finally, the rest of tests (7.40.15, 7.40.16 and 7.40.17), show a quasi-steady state from the beginning of the runs, which could be an indication that oxygen production and consumption occur at similar rates.

The evolution of hydrogen peroxide concentration with time shows two different behaviours as in the previous cases. In runs 7.40.15, 7.40.16, 7.40.18, the concentration of hydrogen peroxide increases initially to reach a steady state. For the rest of the runs, concentrations of hydrogen peroxide decrease with time to reach the same steady-state concentrations. It is important to notice that the final concentrations measured in experiment 7.40.15 are nearly one order of magnitude lower than the steady state concentrations measured in the rest of the runs. Once again in these series of tests, hydrogen and oxygen concentrations are higher than hydrogen peroxide concentrations.

3.1.3 Experiments in 1 mM NaCl in solution

Five runs were carried out by using a solution composition containing 10 mM of $NaHCO_3$ and 1 mM of NaCl. Hydrogen and oxygen concentrations in the gas phase and hydrogen peroxide concentrations as a function of time are plotted in Figure 4.

A continuous increase of the hydrogen concentrations with time is observed. Measured concentrations are also comparable in all the tests, although a slight difference in the slope can be observed for tests 7.40.11 and 7.40.13 with respect to the other ones. Oxygen concentrations follow a different trend since they increase with time but the final concentrations measured seem to lead up to a steady-state concentration of this species in the system. As in the previous series, we can also differentiate several slopes in the graph indicating different generation rates for this gas. The largest oxygen concentrations are obtained in test 7.40.11, reaching values quite close to the ones measured for hydrogen in the same experiment. Tests 7.40.7 and 7.40.8 reach concentrations around 600 ppm at the end of each run indicating a lower oxygen production with respect to the previous one. Finally, the rest of the tests (7.40.13 and 7.40.14) show very low concentrations of oxygen, with values reaching less than 100 ppm at the end of these runs.

For hydrogen peroxide concentration the only trend observed is their decrease with time leading to a steady state value. As in the previous series, hydrogen peroxide concentrations are lower than the ones measured for oxygen or hydrogen in all the tests.

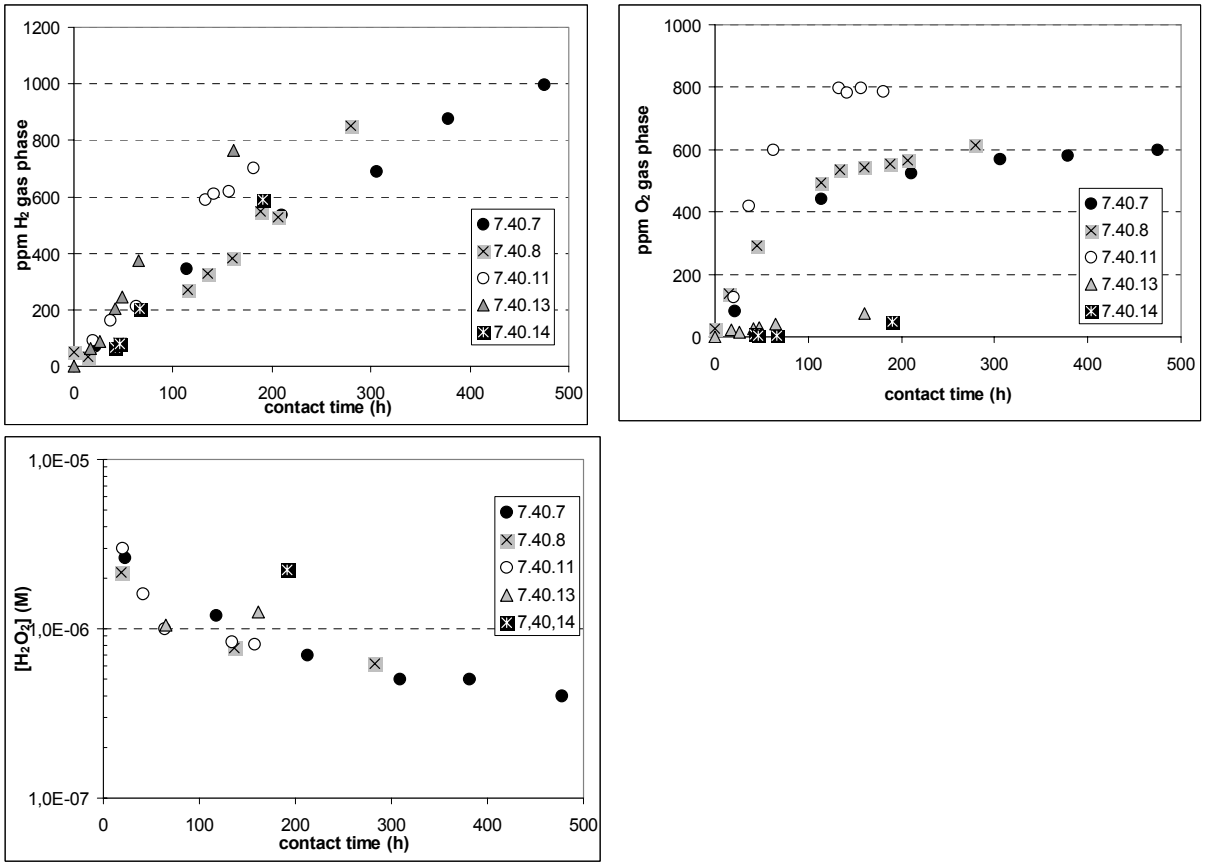

Figure 4. *Concentrations of hydrogen and oxygen in the gas phase and hydrogen peroxide in solution as a function of time. Data gathered at 10 mM $NaHCO_3$ and 1 mM NaCl.*

3.1.4 Experiments in 10 mM NaCl in solution

The only run (7.40.19) carried out by using a solution composition containing 10 mM of $NaHCO_3$ and 10 mM of NaCl is reported in this section. Hydrogen and oxygen concentrations in the gas phase and hydrogen peroxide concentrations are plotted as a function of time in Figure 5.

Hydrogen and oxygen measurements follow the same trend, a continuous increase of their concentrations with time although the different slopes observed in the plot indicate a different gas production. On the contrary, hydrogen peroxide shows an initial increase of its concentration with time to reach a steady state. Hydrogen peroxide concentrations measured in solution are lower than the total hydrogen and oxygen production.

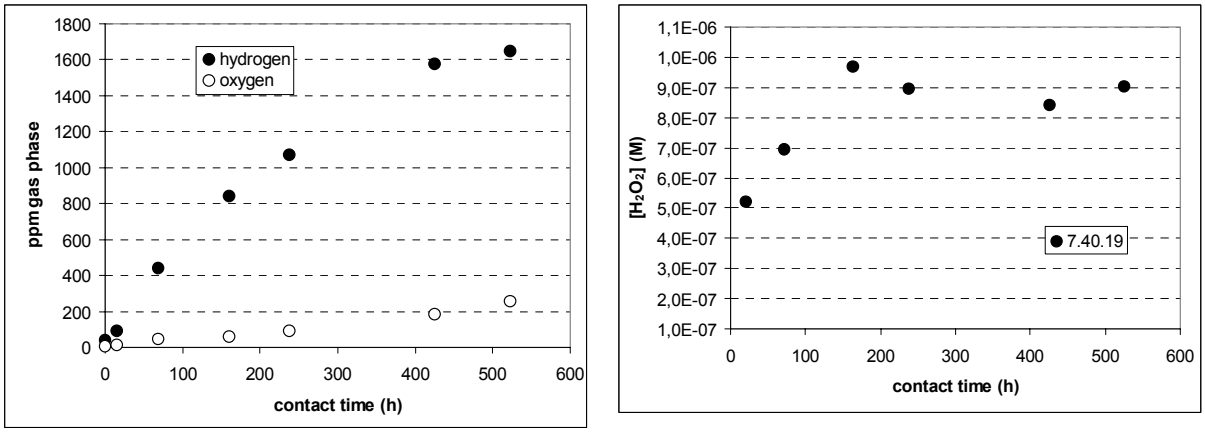

Figure 5. *Concentrations of hydrogen and oxygen in the gas phase and hydrogen peroxide in solution as a function of time. Data gathered at 10 mM $NaHCO_3$ and 10 mM NaCl.*

3.1.5 Effect of solution composition

In order to elucidate the differences in the generation of the different radiolysis products as a function of the water composition we have plotted all the runs in the same graph for hydrogen, oxygen and hydrogen peroxide respectively. These plots are shown in the following figures.

Figure 6 shows the evolution of the concentration of hydrogen with time in the aqueous phase, which is clearly independent of chloride concentration in solution. No clear relationship can be found for oxygen evolution and NaCl concentration and the large scatter would indicate that oxygen concentrations are the dynamic results of a series of processes that affect its consumption (Figure 7).

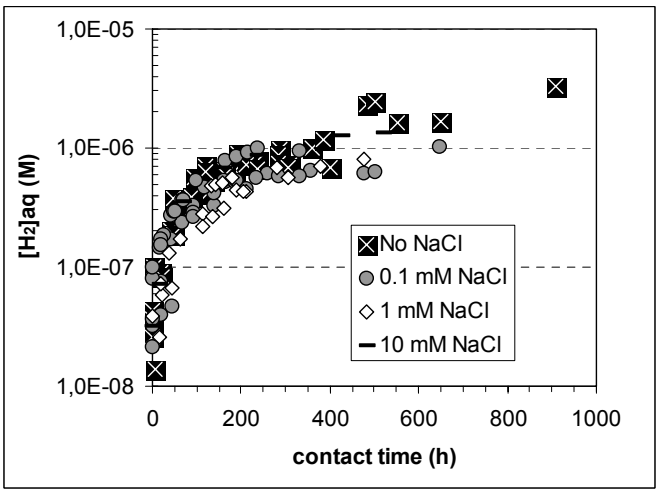

Figure 6. *Hydrogen concentrations in solution as a function of time.*

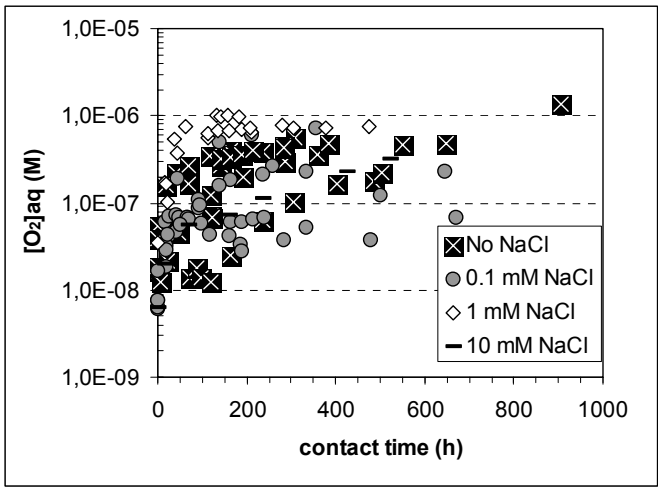

Figure 7. *Oxygen concentrations in solution as a function of time.*

Two different trends are observed for hydrogen peroxide (Figure 8), as well as two differentiated steady-state concentrations. In some of the runs, the steady-state is reached after an initial increase of the concentration with time while in the rest of the leaching tests hydrogen peroxide concentrations decrease from the beginning to reach the same steady-states. With the notable exception of experiment 7.40.15 the steady state concentration of hydrogen peroxide is 3 to 4 times higher in the chloride containing than in chloride free solutions. /Eriksen el al, 1989/ observed no effect of 2 mM Cl^- on the hydrogen peroxide production in α-irradiated 2 mM carbonate solution, thus the data in this work may possibly indicate some passivation of the fuel surface. As it was previously stated /Bruno et al, 1999/ measured hydrogen peroxide concentrations reflected the overall balance between its generation as a radiolysis products at the spent fuel/water interface, its production and recombination reactions determined by the water radiolysis in the bulk solution, its consumption by the UO_2 surface and its decomposition to generate oxygen plus water.

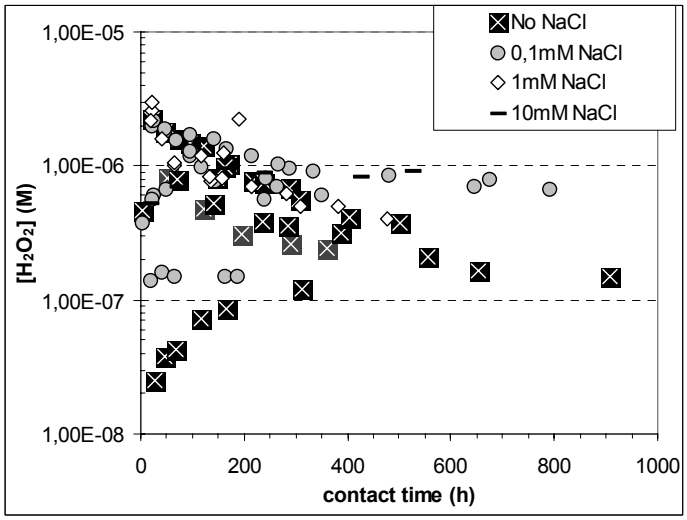

Figure 8. *Hydrogen peroxide concentrations as a function of time.*

3.2 Radionuclide concentration in solution

The solution concentrations of the different radionuclides measured at different time intervals are given in the following graphs. In this case, experiments are grouped by elements and separated as a function of the initial chloride content in the test solution.

3.2.1 Uranium

The concentration of uranium in solution increases with time in all the tests, the only different trend is given in run 7.40.15 showing a decrease of the concentration of U with time (Figure 9). This decrease indicates that another mechanism, probably a precipitation process is governing the release of this radionuclide in this test.

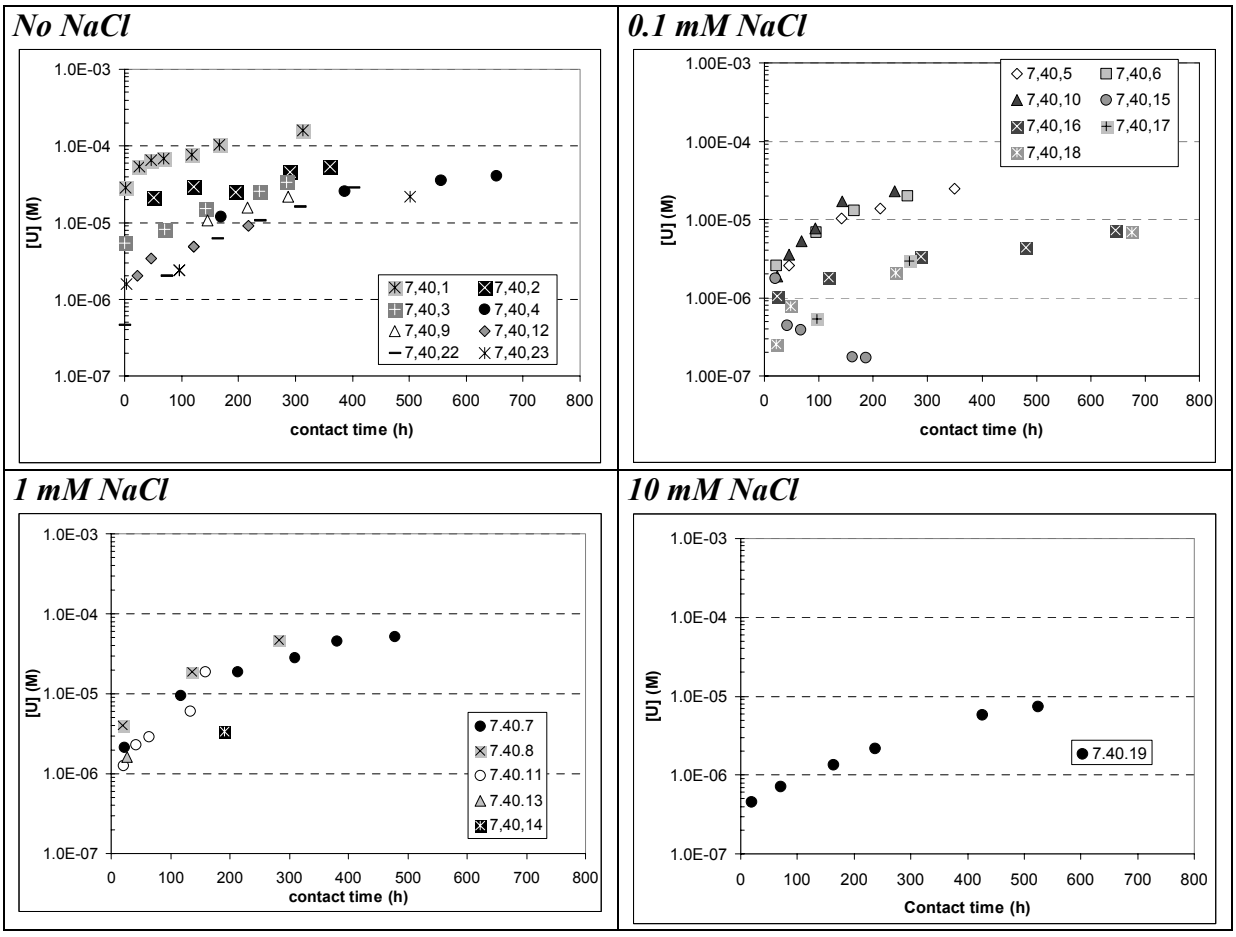

Figure 9. *Evolution of uranium concentrations with time.*

The uranium concentration in the first run (7.40.1) is always higher than the concentration measured in the successive tests showing the different nature of the contacting surface. The fact that this initial release is consistently measured for all redox dependent nuclides (as it is shown later on) and with particular emphasis in the case of uranium should indicate that this is due to the dissolution of a partly oxidised surface layer of the spent fuel sample. By looking at the uranium concentration in tests 7.40.2 and 7.40.3, we can also see a slightly larger release in these tests with respect to the successive ones, indicating that these experiments are still influenced by the dissolution of the initially oxidised surface layer.

The measured concentrations of uranium fall in the same range (10^{-6} M to 10^{-4} M), in all the series and it does not seem to be any dependence of their release on the initial chloride content of the solution.

The series with 0.1 mM of chloride show two distinctive trends in the release of the major component of the matrix, giving concentrations around one order of magnitude different at the same time interval. These differences are also observed in the oxygen gas evolution with time (Figure 3). We can observe that the larger oxygen production is accompanied by a larger uranium release.

These differences might also be attributed to experimental or analytical errors since all the measured data are in the same range as the one measured in the other experimental series. All these statements will be explored later on.

3.2.2 Plutonium

Plutonium concentrations in solution reach a steady state value at short contact times indicating that the precipitation of a secondary Pu solid phase controls its behaviour in these tests (Figure 10). The only test that leads to a different steady state is the first one (7.40.1). The steady state reached is one order of magnitude higher than the one reached in the rest. This difference was explained in /Bruno et al, 1999/ by the larger release in the first run with respect to the other ones, leading to a higher concentration of Pu in solution that should be governed by the formation of colloidal particles.

In runs 7.40.2 and 7.40.3, this steady state is reached after an initial sharp increase followed by a decrease of the concentration with time. In the other ones, plutonium concentrations increase from the beginning of the experiment until reaching the same steady state. The initial sharp increase observed in runs 7.40.2 and 7.40.3 can also be explained by the major release of the partially oxidised fresh fuel sample, according to the slightly larger release of uranium (Figure 9).

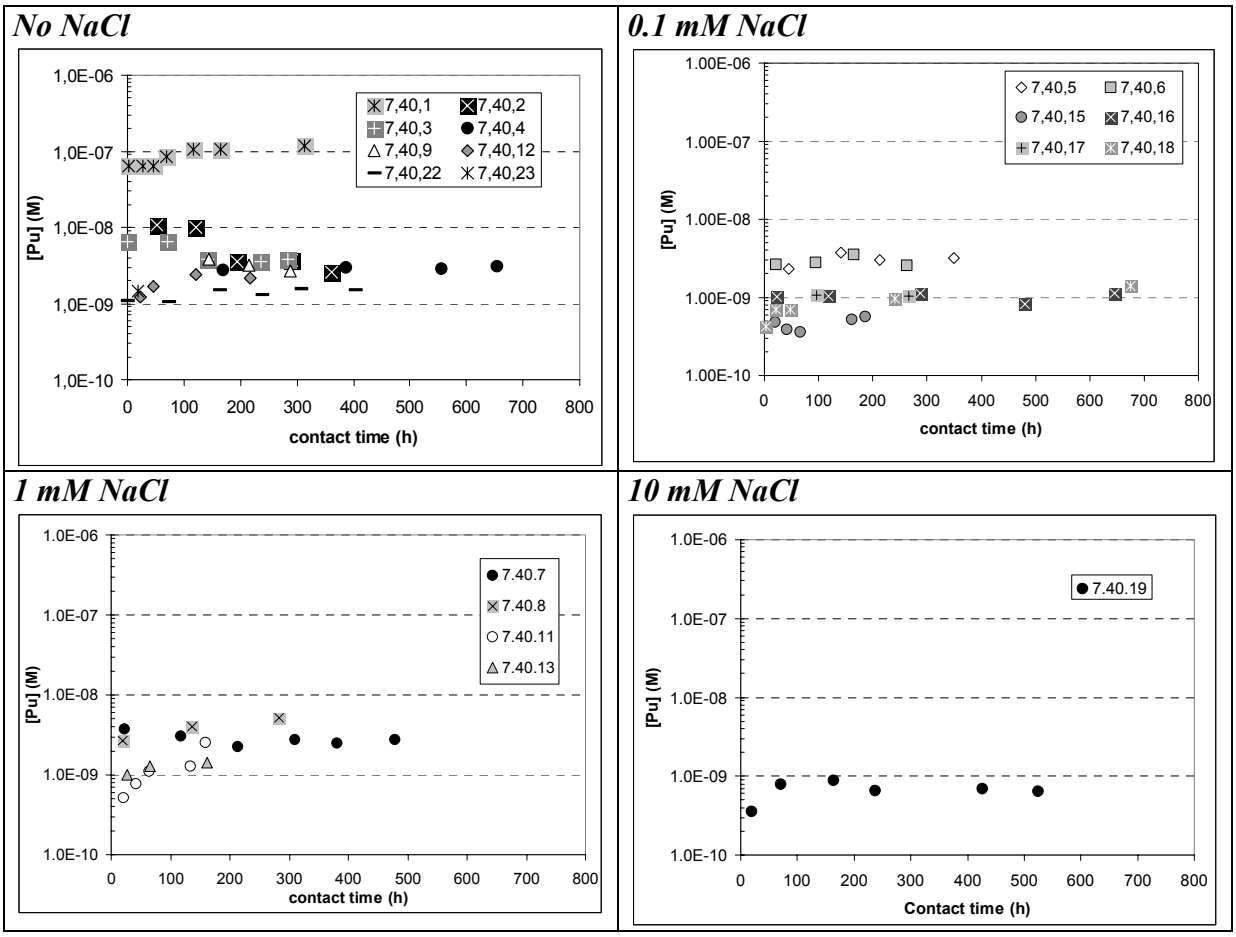

Figure 10. *Evolution of plutonium concentrations with time.*

No dependence of the steady state concentrations on the initial concentration of chloride in the solution is observed. The concentrations in most of the tests reach steady state values ranging from $8 \cdot 10^{-10}$ M to $3 \cdot 10^{-9}$ M, the variation falls within the range of experimental uncertainty.

3.2.3 Neptunium

Neptunium concentrations in solution follow the same trend as uranium; the concentration increases in solution with time in each experimental test (Figure 11). Two ranges of concentrations might be differentiated. The first one with values around 10^{-8} M and the second one with values one order of magnitude lower. No steady state is reached in this case.

The higher or lower neptunium release agrees fairly well with the release of the major component of the matrix (Figure 9), see runs 7.40.2, 7.40.6, 7.40.8, 7.40.16 and 7.40.19 for comparison. This parallelism indicates that a congruent co-dissolution process of Np from the matrix might be occurring in the system.

No difference in the behaviour of neptunium as a function of the chloride content in solution is observed. The very different behaviour of run 7.40.7 with respect to the other ones with 1 mM of NaCl in solution is somewhat strange since it has not been observed for the other elements what is an indication that these results could be a consequence of some analytical disturbance.

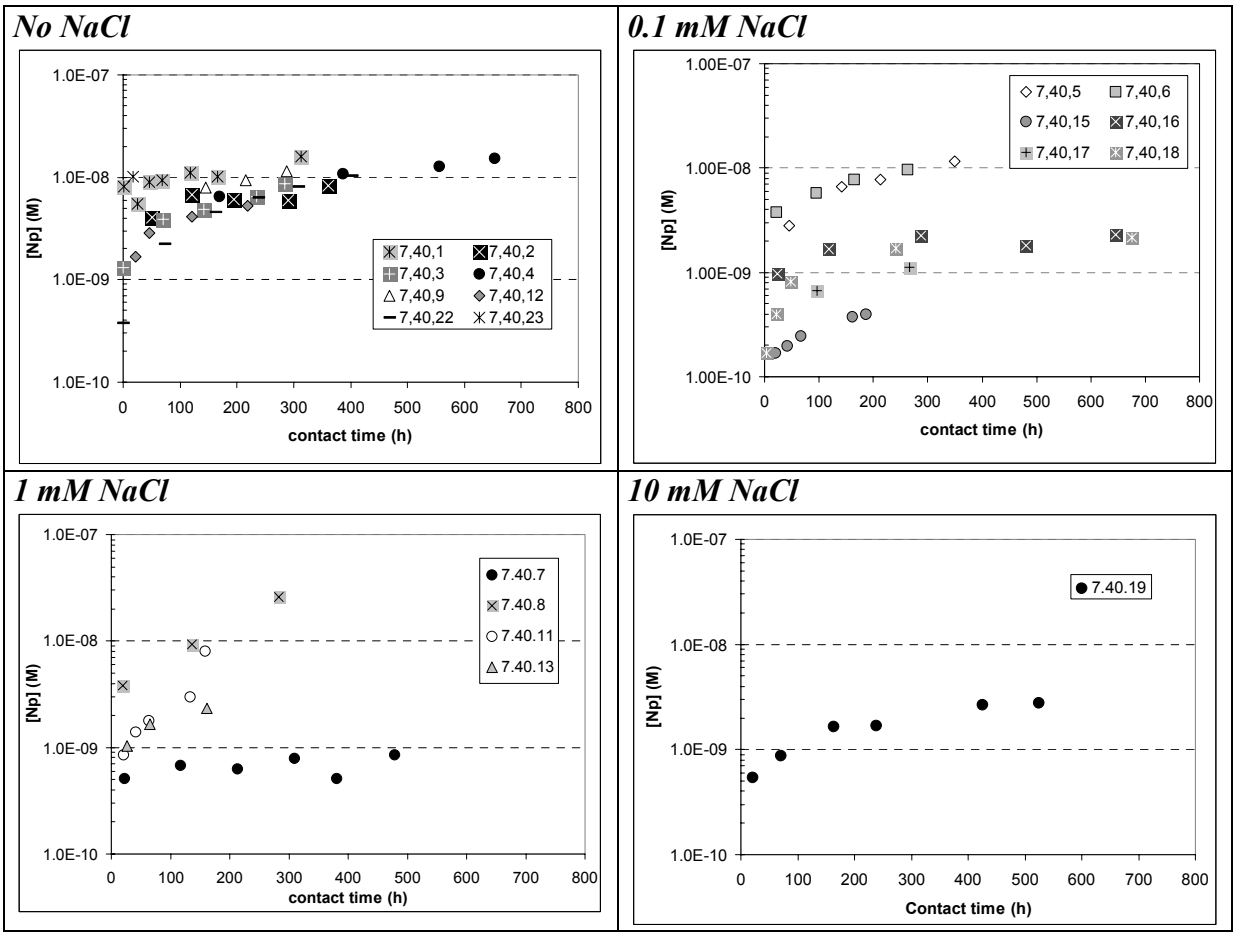

Figure 11. *Evolution of neptunium concentrations with time.*

3.2.4 Strontium

The evolution of strontium concentration with time shows the same trend as for uranium (Figure 12). Again, the measured strontium concentrations in the first run were higher than in the other three showing the same pattern as uranium. In addition, the successive runs show the same pattern as uranium and neptunium since the strontium release decreases according to the lower uranium release, see runs 7.40.2, 7.40.6 and 7.40.16 for comparison. This parallelism could indicate a co-dissolution process of strontium with uranium, the major component of the fuel sample.

As in the previous case, two trends may be distinguished in tests carried out with 0.1 mM of chloride in solution, which is a new indication of the parallelism with the behaviour of U and Np. In some of the runs, strontium concentrations seem to reach a steady state, indicating that some secondary solid phase could precipitate. This possibility will be studied later on.

No difference in the release behaviour as a function of the chloride content in solution is observed.

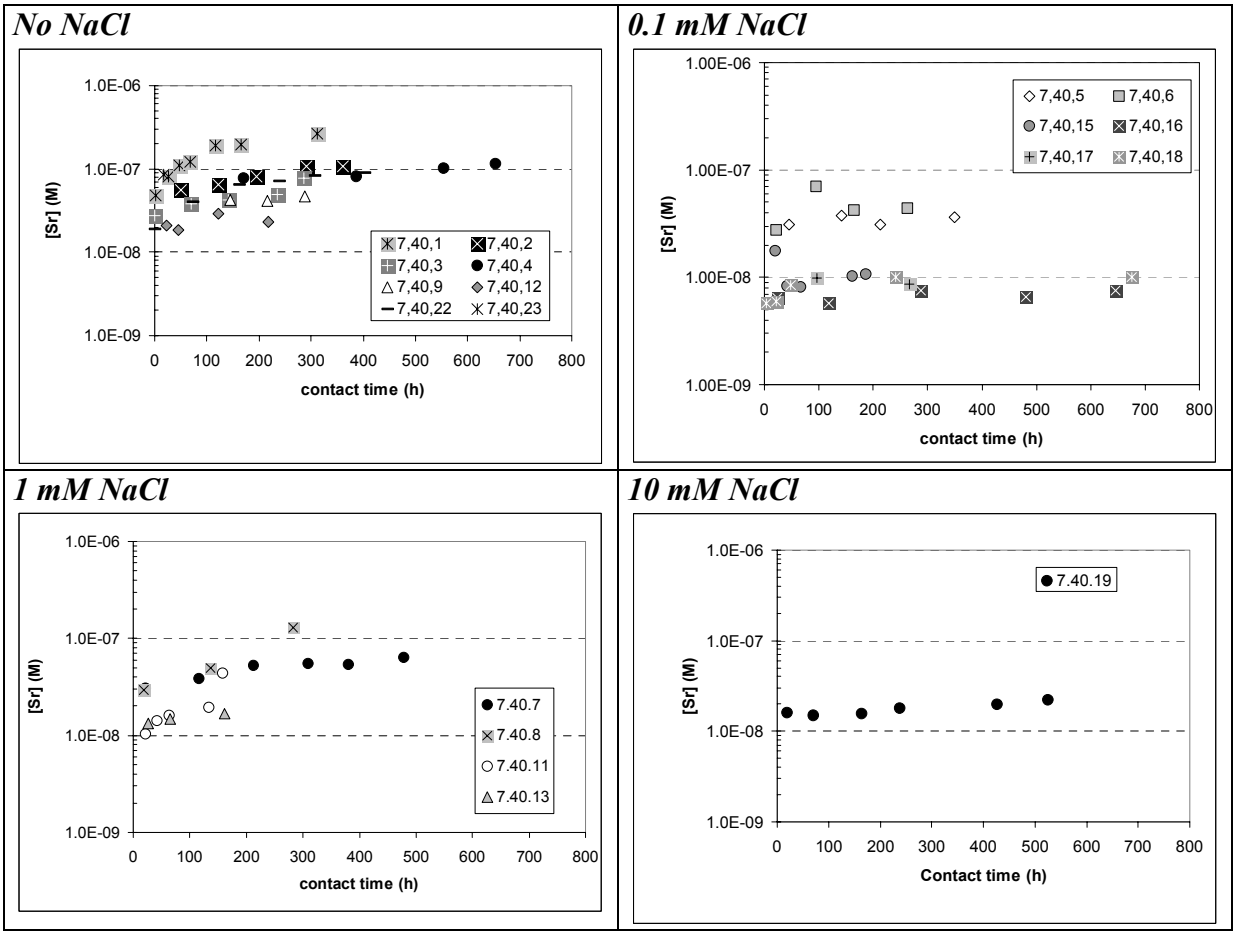

Figure 12. *Evolution of strontium concentrations with time.*

3.2.5 Caesium

The evolution of caesium concentrations with time shows the same trend as uranium (Figure 13). The release of caesium is larger in the first test, and decreases in the following ones, which is in agreement with the increased concentration of this radionuclide at the fuel surface. This behaviour is illustrated when comparing the data from tests 7.40.1, 7.40.2, 7.40.3, 7.40.4, 7.40.5 where it is noticed the successive decrease of the release rates, and consequently of the caesium concentrations in solution.

The two release rates observed in the series with 0.1 mM of chloride in solution agree with the trends previously discussed for the other elements (Sr, Np). This is an indication that after the initial faster release of the caesium located at the grain boundaries, the release of this element is governed by a co-dissolution process with the major component of the fuel matrix, uranium.

No marked difference in the release behaviour with the chloride content in solution is observed.

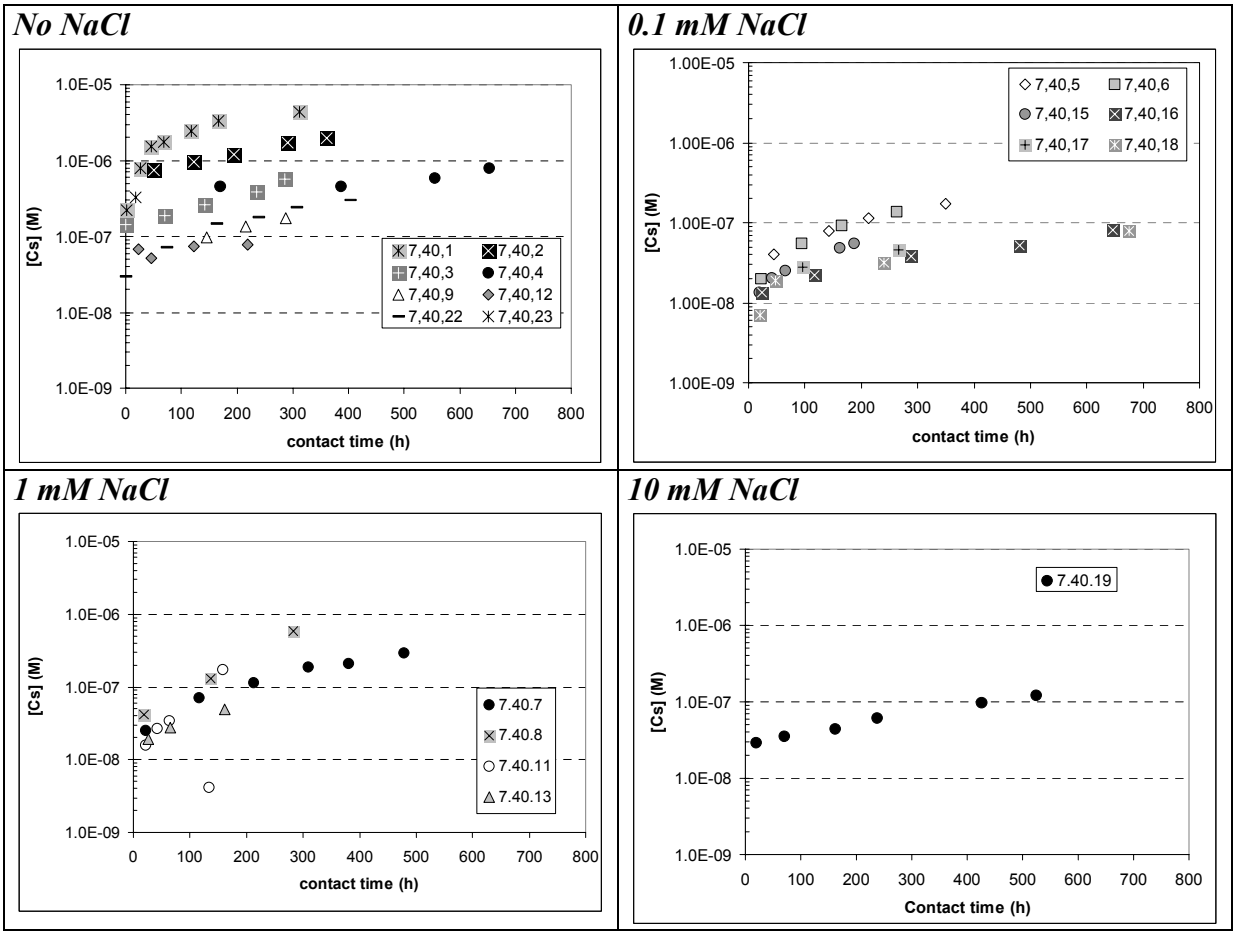

Figure 13. *Evolution of caesium concentrations with time.*

3.2.6 Molybdenum

Molybdenum concentrations with time show the same trend as uranium (Figure 14). Concentrations in the first runs are slightly larger than in the successive ones, indicating again a major release given by the dissolution of the oxidised fuel surface. The similarity in their behaviour could also indicate a co-dissolution process with the major component of the system governing the release of these radionuclides from the fuel.

As in the previous cases, small differences in series with 0.1 mM of chloride in the system are observed corroborating again the previous statement.

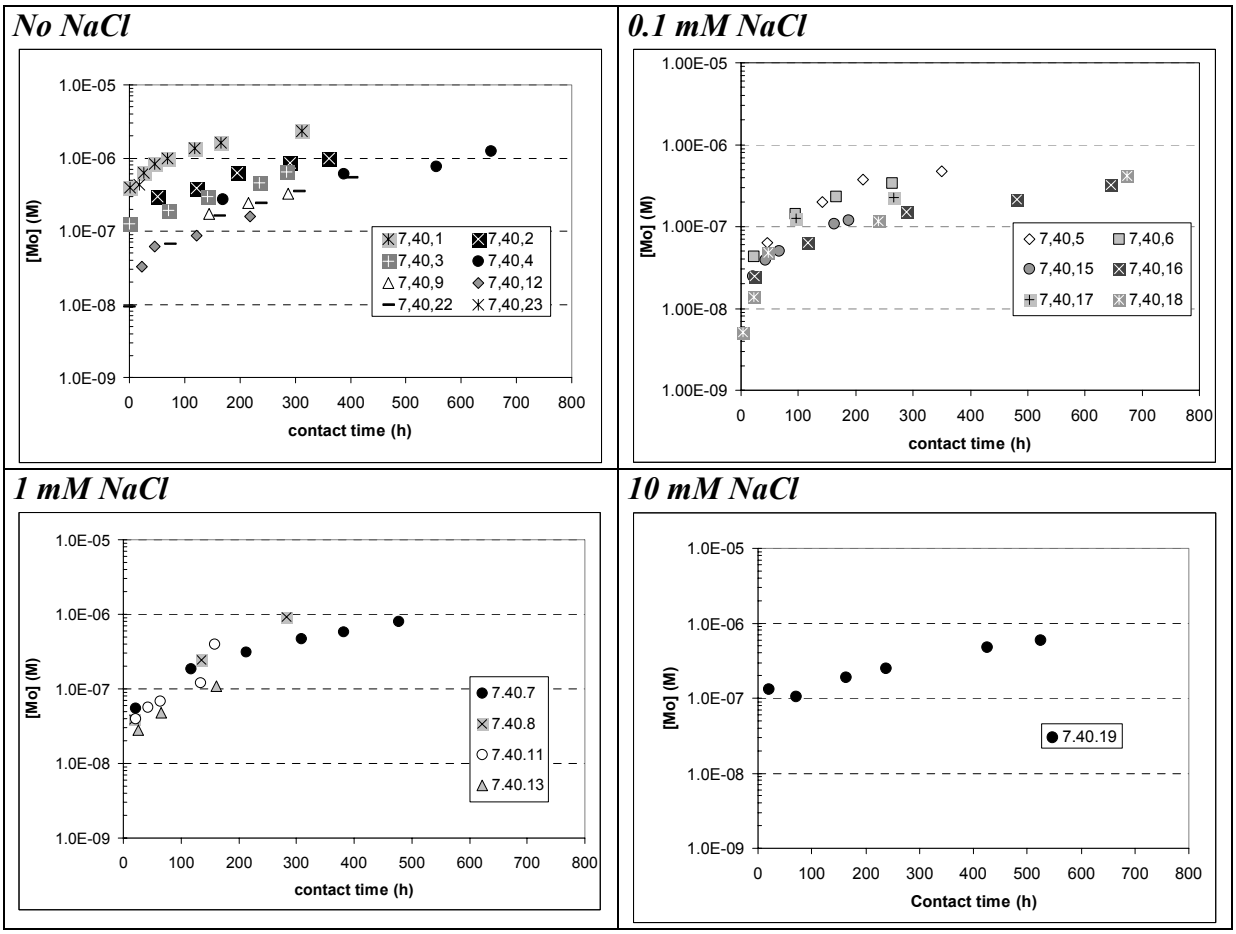

Figure 14. *Evolution of molybdenum concentrations with time.*

3.2.7 Technetium

Technetium concentrations with time follow the same pattern as molybdenum, therefore, this radionuclide shows the same behaviour as uranium (Figure 15). As in the previous cases, the similarity in their behaviour could also indicate a co-dissolution process with the major component of the system governing the release of these radionuclides from the fuel. The concentrations of molybdenum are slightly larger than the technetium ones in all the runs. Neither molybdenum nor technetium show differences depending on the chloride content of the solution.

Technetium concentrations also show slightly different releases for tests carried out with 0.1 mM NaCl of solution.

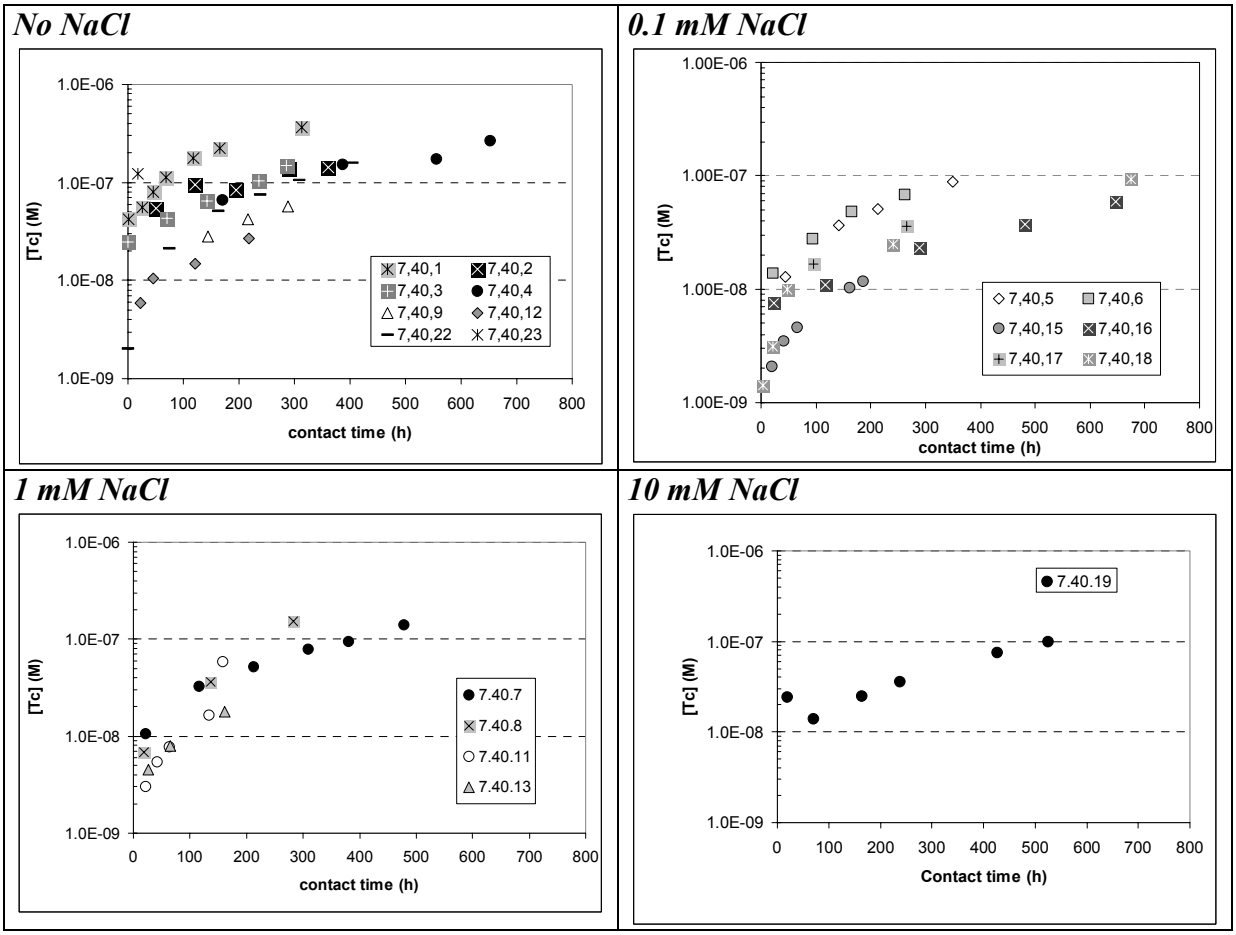

Figure 15. *Evolution of technetium concentrations with time.*

3.2.8 Yttrium

The evolution of yttrium concentration with contact time is different to the evolution of the major component of the fuel (Figure 16), reaching in most cases a steady state at short contact times. This different behaviour indicates that this radionuclide is solubility controlled. The pattern followed by this element is quite similar to the one previously explained for plutonium. The first run (7.40.1) leads to larger yttrium concentrations in solution probably given by the initial release of the oxidised fuel surface. In the successive runs (7.40.2 and 7.40.3), this steady state is reached after the initial sharp increase followed by a decrease of the concentration with time. In the other ones, the steady state is observed from the first data point available.

A slight difference is also observed between runs in series with 0.1 mM of chloride. Taking into account that in this case the concentration in solution is thermodynamically controlled, the difference in the concentrations could be explained by a analytical problem, in such case, the same reasoning may be applied for the previous elements. However, this effect will be explored later on.

Measured data do not show any dependence on the initial chloride content of the solution, with steady state concentrations ranging from 10^{-9} to $5 \cdot 10^{-9}$ M.

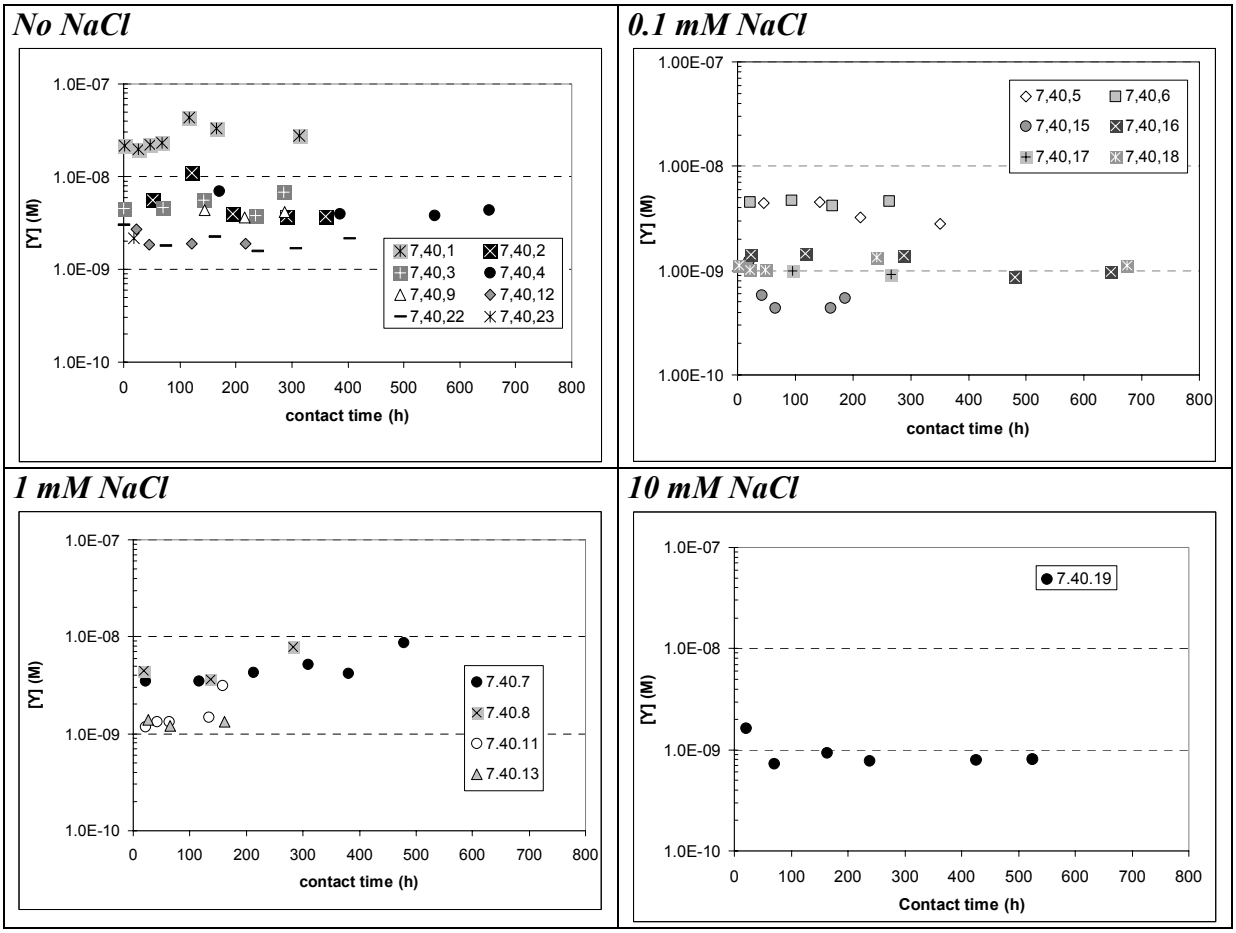

Figure 16. *Evolution of yttrium concentrations with time.*

3.2.9 Neodymium

The same reasoning as the one presented for yttrium may be applied to explain dissolution data of neodymium (Figure 17). On the other hand, the concentrations reached by both elements are very similar despite their different content in the fuel sample. Nd content is some 8 times larger in the fuel than Y.

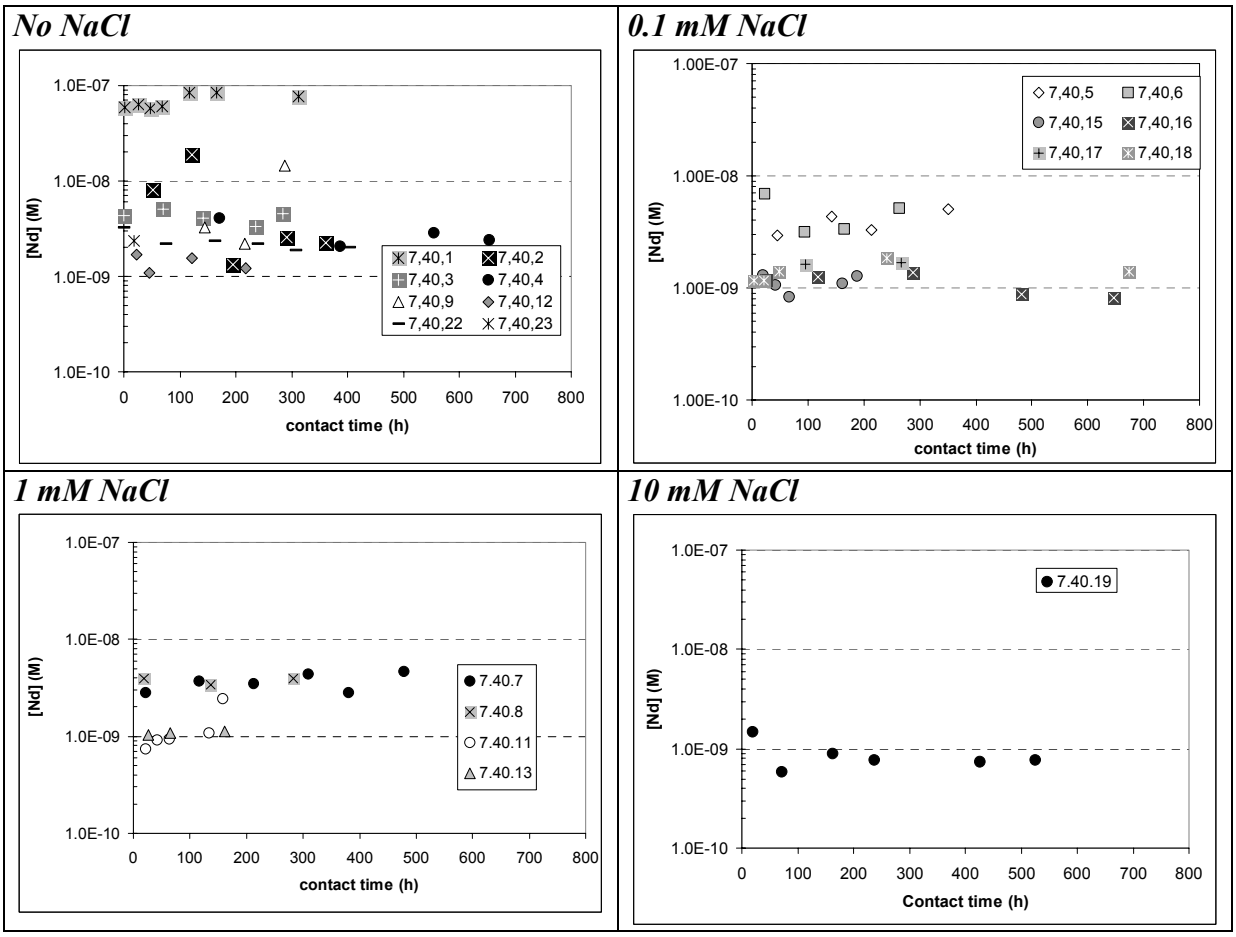

Figure 17. *Evolution of neodymium concentrations with time.*

4 Discussion

4.1 Literature review on radiolysis products

4.1.1 The role of hydrogen

The dissolution rate of UO_2 in aqueous solutions as well as the release rate of radionuclides in the fuel depends on the degree of surface oxidation, which is governed by the solution redox conditions /Sunder et al, 1992/. Although groundwaters at the expected depth of a deep disposal are generally reducing, redox conditions near the fuel surface may be altered by the radiolysis of water. One important factor affecting spent fuel dissolution may be the production of reactive species by the radiolytic decomposition of water. Radiolysis of water produces both molecular (H_2O_2, H_2) and radical ($\cdot OH$, $O_2\cdot^-$, $HO_2\cdot$, e_{aq}^-, $H\cdot$) products. The production of oxidising agents (H_2O_2, $\cdot OH$, ..) by radiolysis is accompanied by the production of an equivalent amount of reducing species (H_2, …).

Molecular hydrogen is formed directly and by recombination of $H\cdot$ radicals on radiolysis of water and, being relatively stable, tends to accumulate in the system during irradiation. /Sunder et al, 1990/ showed that at temperatures of 100ºC, the presence of dissolved H_2 in distilled and deoxygenated water reduced the effect of water radiolysis on oxidation and dissolution of UO_2. These results are consistent with those of /King et al, 1999/. Working at a pressure of 5 MPa he concluded that H_2 not only consumes the oxidants produced by gamma irradiation but also reduces the surface, presumably through the reaction between the surface and reducing radiolysis products such as e^-(aq) or $H\cdot$. The effects of H_2 have been found to be kinetically slow and persistent, retarding the subsequent re-oxidation of the surface after the H_2 atmosphere has been replaced by Ar. The authors suggested that radiolytically produced reductants participate in homogeneous reactions in solution with radiolytic oxidants and in heterogeneous reactions on the UO_2 surface, most likely at reactive grain-boundary sites.

/Röllin et al, 2001/ investigated the dissolution rate of UO_2 fuel with H_2(g) saturated solutions observing a decrease of the dissolution rate of U and other redox sensitive elements. The authors argue that this decrease may be due either to a catalytic effect of the UO_2 surface on hydrogen or to the hydrogen activation by the radiolytic effect causing an increase of the hydrogen radical concentration.

As /King et al, 1999/ reported, there is evidence to suggest that radiation induced UO_2 oxidation is suppressed by high H_2 concentrations at ambient temperature and by low H_2 concentrations at elevated temperature. The exact dependence of the process on hydrogen concentration and ambient temperature, however, is unknown. Besides, the authors observed that the amount of H_2 produced by radiolysis of the solution in short-term experiments was insufficient to suppress oxidation at room temperature. On the other hand, H_2 as the reducing molecular product is relatively inert at temperature below 100ºC. Hence, it is expected that the water radiolysis will cause oxidising conditions near the fuel surface, even in a disposal vault where groundwater is generally reducing /Sattonay et al, 2001; Sunder and Shoesmith, 1991/. The experiments to be modelled in this report are obtained at low hydrogen pressures and at ambient temperature, so it is expected that the hydrogen gas produced will be inert under such conditions.

4.1.2 The role of carbonate

/Andreozzi et al, 1999/ studied the effect of carbonate on the water radiolysis. Carbonate in addition to being a complexing agent acts as a scavenger for OH radicals. The carbonate radical ion is formed according to the following reactions and rate constants:

$HCO_3^- + \cdot OH \Rightarrow CO_3^{-}\cdot + H_2O \qquad k_{41} = 1.7\times10^7\ M^{-1}s^{-1}$ (4-1)

$CO_3^{2-} + OH\cdot \Rightarrow CO_3^{-}\cdot + OH^- \qquad k_{42} = 4.9\times10^8\ M^{-1}s^{-1}$ (4-2)

$O^- + CO_3^{2-} \Rightarrow CO_3^{-}\cdot + 2OH^- \qquad$ in highly alkaline solutions (4-3)

$CO_3^{-}\cdot$ being negatively charged and with a lower reduction potential than $OH\cdot$ is expected to be less reactive than $OH\cdot$.

/Behar et al, 1969/ found that the basic form of hydroxyl radical O^- contributes little to the production of the carbonate radical ($CO_3^{-}\cdot$) even up to pH 14. Reactions of the carbonate radical with hydrogen peroxide were observed in their work, and the following mechanism governs the disappearance of the carbonate radical in reaction with hydrogen peroxide:

$CO_3^{-}\cdot + H_2O_2 \Rightarrow$ products (4-4)

$CO_3^{-}\cdot + HO_2^- \Rightarrow$ products (4-5)

The product of the reaction: $CO_3^{-}\cdot + O_2^- \Rightarrow$ is assumed to be CO_5^{2-}, having a half-life time of several seconds.

4.1.3 The role of chloride

Chloride may participate in a large number of radiolysis reactions /Sunder and Christensen, 1993/. Most of the additional species formed in Cl^- containing solution (such as ClO_2, Cl_2,…) are oxidants rather than reductants.

/Kelm, 2001/ analysed ClO^-, ClO_2^- and ClO_3^- in solution after a radiolysis experiment where a UO_2 pellet doped with Pu was put in contact with 5 M NaCl solution. The analyses detected ClO^- and ClO_3^- in solution as chlorine containing species, apart of the chloride ion. The ClO_2^- concentrations remained near the detection limit around 10^{-5} M. Moreover, the yields of H_2 and O_2 were independent of pH, but the yield of ClO^- decreased with pH in favour of ClO_3^-. In previous experiments, the same authors /Kelm et al, 1999; Kelm and Bohnert, 2000a,b/ showed that the main products formed by gamma radiolysis from NaCl brines at ambient temperature are H_2, O_2 and ClO_3^-, produced proportionally to the adsorbed dose. From these experiments, we should expect that the main final chlorine products formed in the NaCl solutions are ClO_3^- and ClO^-.

/Ershov et al, 2000/ studied the reactions between e^-_{aq} and $\cdot OH$ or ClO_3^- in aqueous solution. The authors studied the competition between ClO_3^- and CO_3^{2-} for the hydroxyl radical and noticed that in a solution containing hydroxyl radical and CO_3^{2-}, the addition of 0.25 M $NaClO_3$ had no effect on the reaction between hydroxyl and CO_3^{2-} radicals ($\cdot OH + CO_3^{2-} \Rightarrow OH^- + CO_3^{-}\cdot$). The yield of the $CO_3^{-}\cdot$ radical ion and its formation kinetics were the same, with and without the addition of ClO_3^-. This is in agreement with the results reported by

/Domae et al, 1994/ that the ·OH radical does not react at all with the ClO_3^- ion, even in concentrated solutions up to 5 M $NaClO_3$. /Ershov et al, 2000/ concluded that the oxidation of the ClO_3^- ion by the ·OH radical is a rather unfavourable process in neutral or alkaline solutions, and this conclusion is in agreement with the results obtained by /Kelm and Bohnert, 2000a, 2000b, 2001/.

Considering now a system with low Cl^- concentration. The oxidation of Cl^- by the ·OH radical is given by the following reactions and rate constants /Jayson et al, 1973/

$$Cl^- + \cdot OH \Rightarrow ClOH^- \qquad k_{46} = 4\times10^9\ M^{-1}s^{-1} \qquad (4\text{-}6)$$

$$ClOH^- \Rightarrow \cdot OH + Cl^- \qquad k_{47} = 6.1\times10^9\ M^{-1}s^{-1} \qquad (4\text{-}7)$$

$$ClOH^- + H^+ \Leftrightarrow \cdot Cl + H_2O \qquad k_{48} = 2.1\times10^{10}\ M^{-1}s^{-1} \qquad (4\text{-}8)$$

$$\cdot Cl + Cl^- \Leftrightarrow Cl_2^- \qquad k_{49} = 2.1\times10^{10}\ M^{-1}s^{-1} \qquad (4\text{-}9)$$

$$ClOH^- + Cl^- \Leftrightarrow Cl_2^- + OH^- \qquad k_{410} = 9\times10^4\ M^{-1}s^{-1} \qquad (4\text{-}10)$$

Assuming equilibria (4-8), (4-9) and (4-10) to be favoured to the right we can estimate the initial fraction of ·OH radicals oxidising Cl^- from reactions (4-1) to (4-10).

$$-d(ClOH^-)/dt = (4\times10^9/6.1\times10^9) \times [Cl^-] \times (2.1\times10^{10}[H^+] + 9\times10^4[Cl^-])$$

$$d(CO_3^-)/dt = (1.7\times10^7[HCO_3^-] + 4.9\times10^8[CO_3^{2-}])$$

The highest Cl^- concentration used in this work is 10 mM, the carbonate concentration was 10 mM and pH approximately 8. The highest fraction ·OH radicals reacting to give oxidised Cl^- species is thus estimated to be $1.3/1.7\cdot10^5$.

Accordingly, the yield of the carbonate radical CO_3^- should be constant within the range of Cl^- concentrations used in this work and the concentration of oxidised chloride containing species is expected to be very low.

4.2 Electron balance

As we have previously mentioned, a equal number of reducing species will accompany the production of oxidant species by radiolysis. In order to check the electron balance of the systems under study we have used the analytical data available from the experimental results. Therefore we have considered as a first step that water radiolysis products, i.e. hydrogen, oxygen and hydrogen peroxide are the only compounds governing the electron balance in these systems.

Oxygen and hydrogen concentrations in solution have been calculated assuming equilibrium between the aqueous and the gas phase, according to the following equation:

$$[X] = ppm \times 10^{-6} \times K_H^x \qquad (4\text{-}11)$$

where ppm denotes the concentration of either oxygen or hydrogen in the gas phase expressed in ppm in volume and K_H^x stands for the Henry's law constant at 1bar and 25ºC. K_H is equal to $1.26 \cdot 10^{-3}$ mole·dm^{-3} for oxygen and $8.11 \cdot 10^{-4}$ mole·dm^{-3} for hydrogen /Stumm and Morgan, 1981/.

The overall production of oxidants and reductants in each test is reflected in the electron balance (EB) calculated by using the experimental data concerning the observed concentrations of the major oxidising and reducing species. Figure 18 shows the electron balance calculated by considering the hydrogen, oxygen and hydrogen peroxide concentrations measured in the gas and aqueous phases according to the following equation:

$$EB = 2 \times [H_2] - 4 \times [O_2] - 2 \times [H_2O_2] \qquad (4\text{-}12)$$

In most of the experiments there is an excess of radiolytically formed reductants, hydrogen, with respect to the oxidants. This trend is observed independently of the series considered. The electron imbalance indicates that there are other oxidant species contributing to the balance of the system.

Nevertheless, some of these experiments present the opposite effect i.e. a major release of oxidants with respect to hydrogen is observed. This is an unexpected result that may be a consequence of a hydrogen leakage in these experiments.

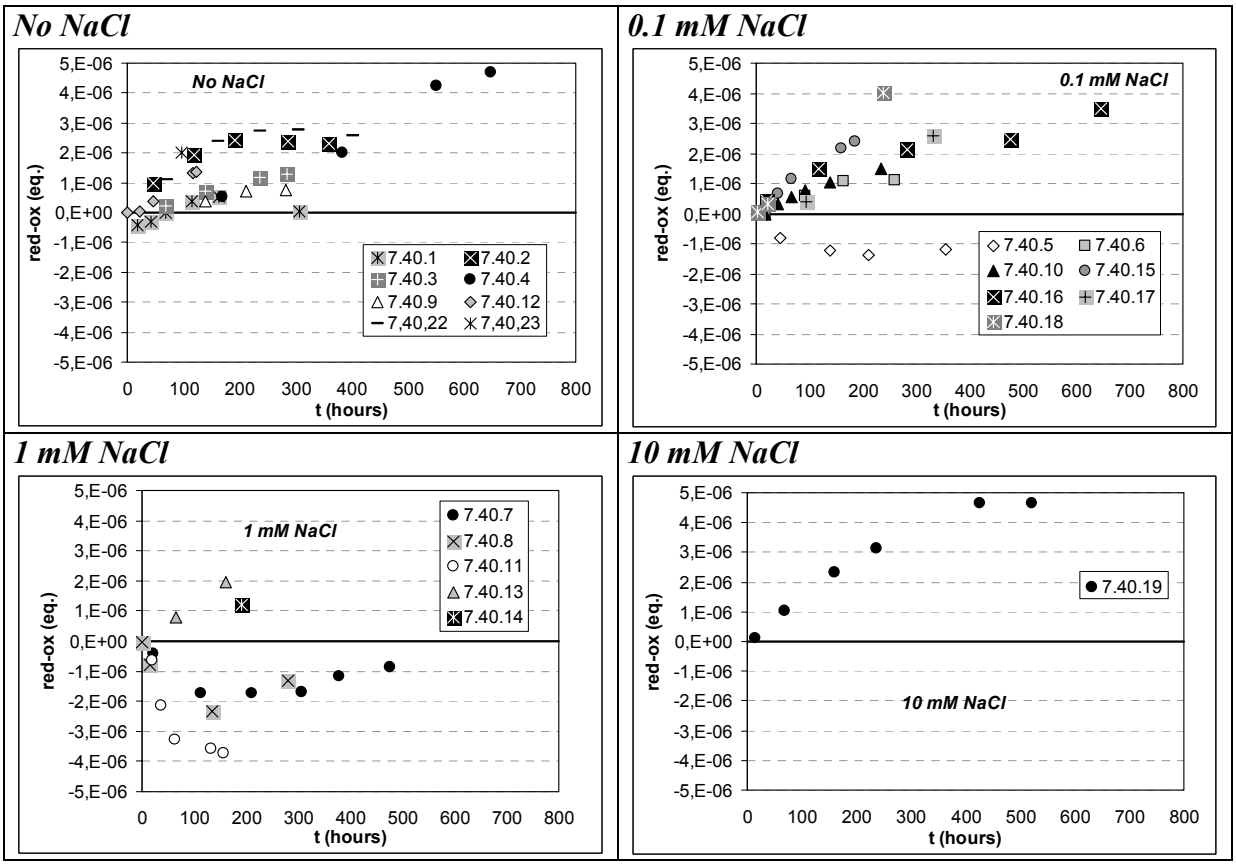

Figure 18. *Electron balance calculated by means of experimental results according to equation (4-14) (see text) as a function of time.*

Experiment 7.40.1 that corresponds to the one using the fresh fuel is the only test showing a nominal electron balance in the system, this is an indication that in this case contributions from other oxidant species are not important.

Figure 19 shows the trend of the different tests studied when including the contribution from the dissolved uranium in the electron balance calculations (equation (4-13)). For these calculations we assume that all the measured uranium is hexavalent, and uranium is released from the fuel matrix as a consequence of the oxidation of UO_2.

$$EB = 2 \times [H_2] - 4 \times [O_2] - 2 \times [H_2O_2] - 2 \times [U(VI)] \qquad (4\text{-}13)$$

For the series without chloride present in the system, the results indicate in general a nominal electron balance of the system. The excess of reductants from the electron balance when considering only the water radiolysis products is compensated by uranium released to the aqueous phase, giving a net balance which in most cases is close to zero (within the analytical uncertainty). This statement has been previously reasoned in /Bruno et al, 1999/. Other redox sensitive fission products like Tc and Mo have been also included in the electron balancing, however the low release to solution of these radionuclides lead us to neglect the effect on the electron balance of these species.

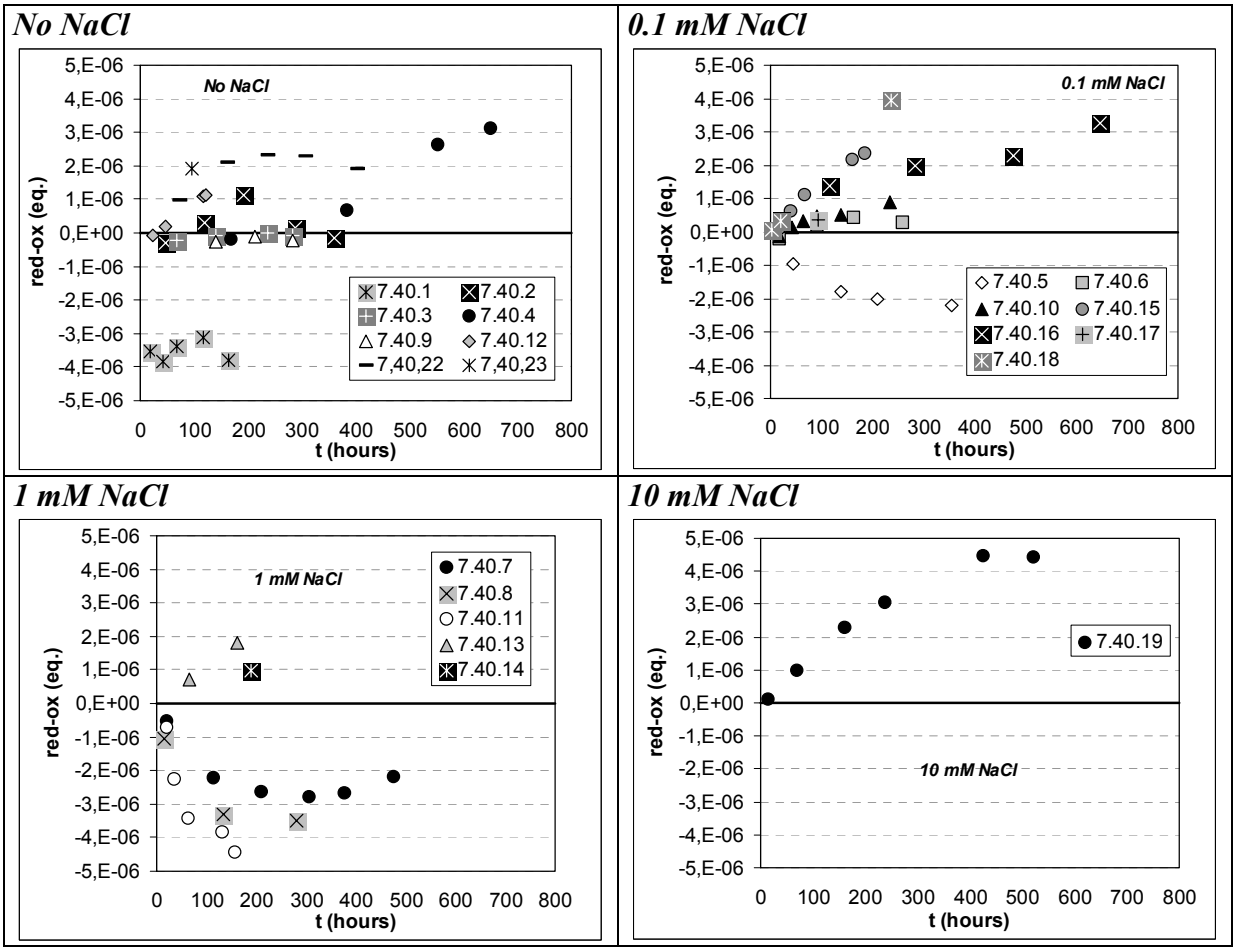

Figure 19. *Electron balance calculated by means of experimental results according to equation (4-15) (see text) as a function of time.*

The electron balance when including the uranium system in data obtained from experiment 7.40.1 shows an excess of oxidant species (Figure 19). As we have noticed, the fuel fragments in this test correspond to a fresh fuel that was not pre-treated to clean the surface, consequently, the surface was probably oxidised. The net electron balance obtained when considering only water radiolysis products (Figure 18) agrees with this statement indicating that no oxidant consumption occurs for uranium oxidation.

When looking at the series containing a given initial chloride content in solution, we do not observe the net electron balance with the inclusion of the uranium system as in the case of the series without chloride. These results indicate that other oxidants present in solution may also have an important contribution for balancing these systems. According to the previous literature review, the presence of chloride in solution should lead to the generation of oxidant species by recombination reactions, i.e. ClO_3^-, ClO_2 etc. Even if the production of oxidised chloride species is low, they may have some influence on the redox balance as the effective G-value for fuel oxidation also is low. Therefore, these oxidant species are probably the compounds contributing to the electron balancing. Unfortunately, there are not experimental data available in order to check this possibility. However, we have verified the amount of oxidant chloride species necessary to balance those systems in order to check if the calculated amounts exceed the initial chloride content in solution. According to the results showed in Figure 19, in all cases the initial chloride content is larger than the concentration of chloride species necessary to balance these systems. Consequently, we might assume a system balanced by these chloride species.

4.3 Estimation of the redox conditions of the experiments

According to the previous modelling, the oxidant species generated by radiolysis of water, mainly oxygen, are scavenged by oxidation of the redox sensitive radionuclides present in the fuel sample. As it has been stated in the introduction, the role of mineral surfaces in poising the redox state of solid/water systems is well documented. This behaviour has been evidenced for uranium in natural systems in Palmottu /Cera et al, 2002/, Cigar lake /Casas and Bruno, 1994/. In addition this role has been also observed when modelling experimental data obtained from spent fuel dissolution experiments reported in the last years /Eriksen et al, 1995; Bruno et al, 1999/.

Given the experimental conditions reported in the present work that are similar to the ones reported in the previous ones, we have established the uranium system for defining the redox couple controlling the redox potential in the aqueous phase according to the following reaction:

$$UO_2(s) + 3HCO_3^- \Leftrightarrow UO_2(CO_3)_3^{4-} + 3H^+ + 2e^- \qquad (4\text{-}14)$$

where the uranyl tri-carbonate aqueous complex is the predominant uranium species in solution under these experimental conditions. In such case, the pe of the system can be expressed as:

$$pe = (\log[UO_2(CO_3)_3^{4-}] - 3 \times pH - 3 \times \log[HCO_3^-] - \log k_{eq}) / 2 \qquad (4\text{-}15)$$

where k_{eq} stands for the equilibrium constant of the above reaction (4-14). Calculated pe's by considering this redox system are shown in the next graphs.

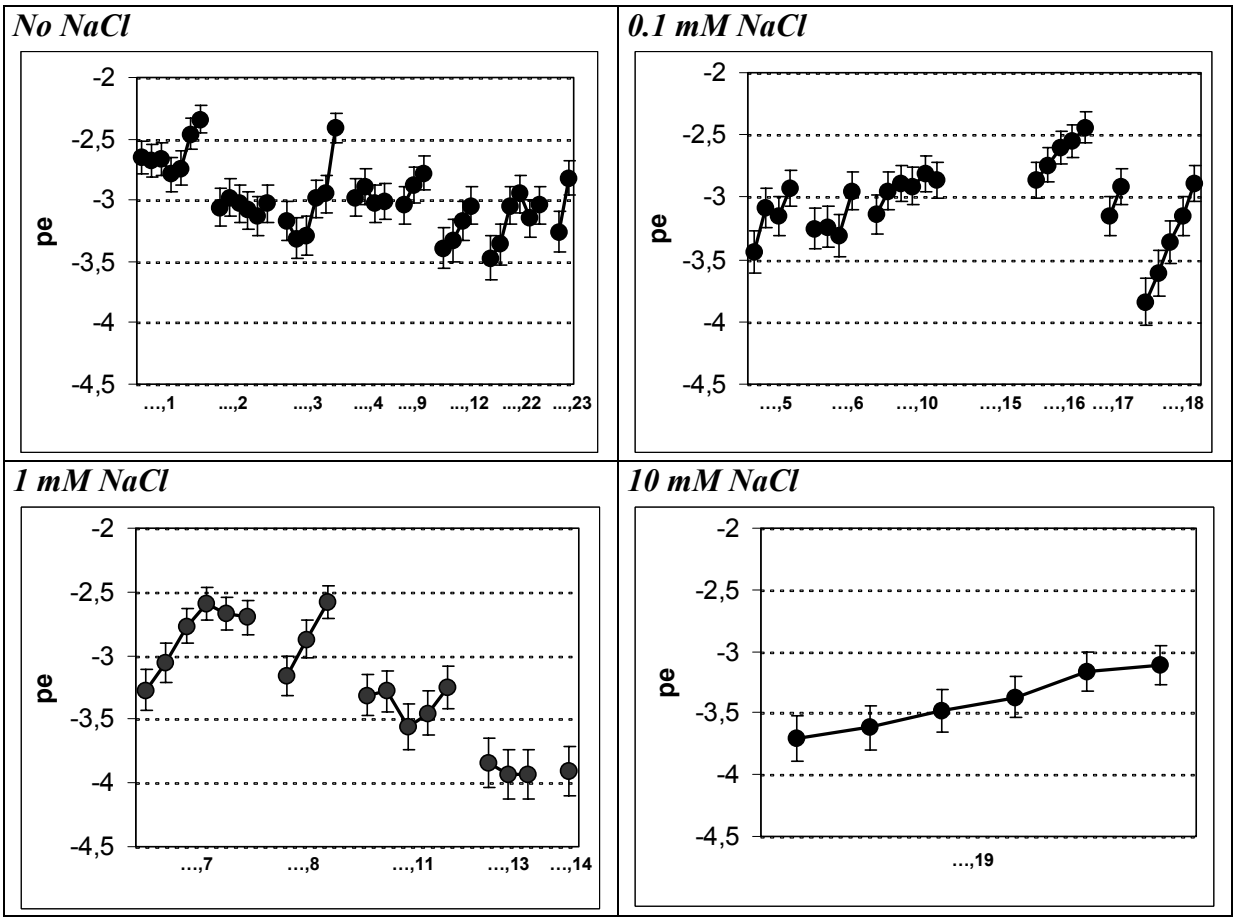

Figure 20. *Calculated pe by using experimental data considering the equilibrium UO_2/U(VI). Error bars correspond to 10% deviation in the ICP measurements of radionuclides in solution /Forsyth and Eklund, 1995/. In each test, time increases from the left to the right.*

Calculated pe's in each experimental point range between –4 and –2.5. The general trend we may observe is a pe increase with time, given by the continuous increase of uranium in the aqueous phase. This trend, as well as the small variability between series led as to think that redox equilibrium is attained in the aqueous phase. Therefore, we may establish a thermodynamic approach controlling the redox state in these experiments. The overall redox state estimated for these experimental systems, given by the mean value obtained from the previous calculations is:

pe = –3.08 ± 0.35

Tc is also a redox sensitive radionuclide contained in the spent fuel matrix. This radionuclide will be located in the solid mainly forming metallic precipitates /Kleykamp, 1988/. Its content in solution has been determined in the present experiments. Consequently, we should establish a thermodynamic equilibrium by means of the following redox pair:

$$Tc(m) + 3H_2O \Leftrightarrow TcO(OH)_2(aq) + 4H^+ + 4e^- \qquad (4\text{-}16)$$

where $TcO(OH)_2(aq)$ is the predominant Tc aqueous species under these experimental conditions.

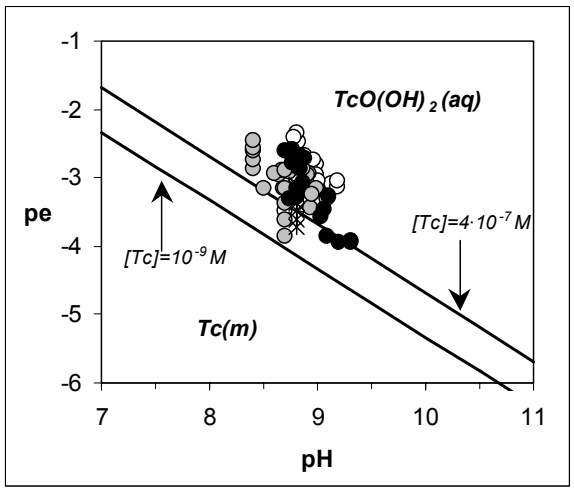

Figure 21. *pe/pH diagram showing the predominance of Tc species in the solid and the aqueous phases according to the previous thermodynamic equilibrium (4-16) (black lines). Filled, empty and grey circles stand for the calculated pe's when considering the redox potential governed by the uranium system.*

The following pe/pH diagram (Figure 21) shows the predominance area of metallic technetium and the hydrolysed species in the aqueous phase for two technetium concentrations in solution standing for the maximum and the minimum concentrations analysed in these experiments. Calculated pe's when considering the redox potential governed by the uranium system are shown in the same plot for comparison.

As we can see in the previous graph, phase boundaries will vary depending on the technetium content in solution as expected. On the other hand, calculated pe's by means of uranium equilibrium are quite close to the phase boundaries accounting for the redox equilibrium of the technetium system. This agreement should lead us to establish that an overall redox equilibrium is attained in the aqueous phase.

4.4 Modelling radionuclide release

4.4.1 Initial dissolution rates

Initial dissolution rates considering a linear dependence of radionuclide concentrations with time have been calculated by using initial solution data from the analysis carried out in all the tests. The results are given in Figure 22.

Dissolution rates for most of the radionuclides follow in general the same trend as the ones of uranium, the exceptions are Pu, and Y and Nd that have not been included in Figure 22. The agreement observed for most of the analysed radionuclides should indicate that the release of these elements is controlled by matrix dissolution. This has been previously observed when studying the evolution of these radionuclides as a function of time. The different trend observed for Pu, Y and Nd is an indication that additional solubility controlling mechanisms operate for these radionuclides from the beginning of the tests given the low solubility limits of the precipitating solid phases under these experimental conditions. These mechanisms have

already been proposed in former analysis of early contact times of very long time leaching experiments /Bruno et al, 1998/.

Initial dissolution rates have been normalised with respect to U according to the inventory ratio, the results are given in Figure 23.

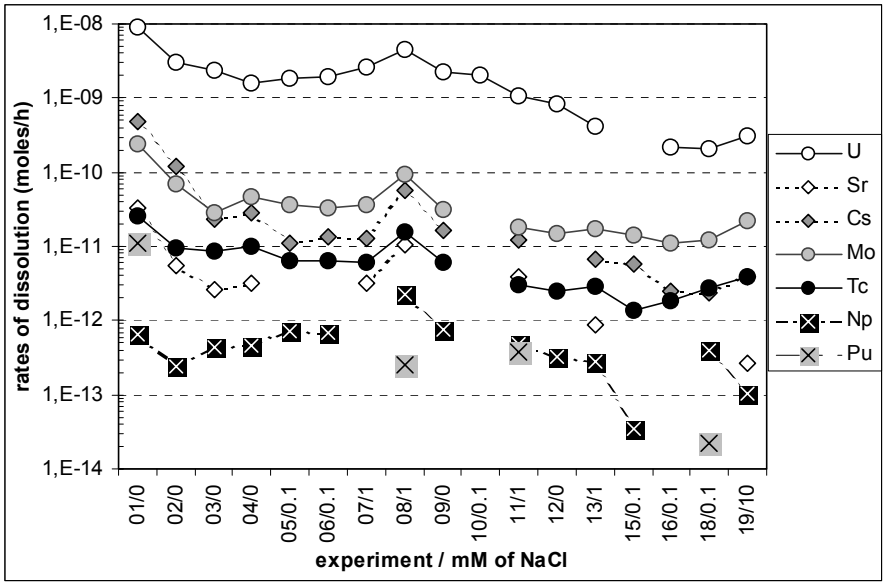

Figure 22. *Radionuclide initial dissolution rates in all the tests. X axis indicates the test number and the initial chloride content.*

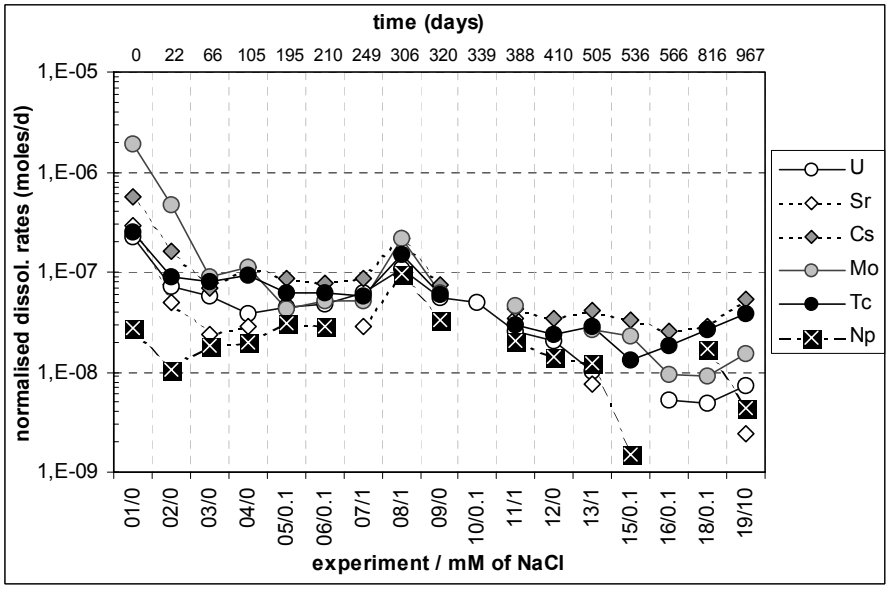

Figure 23. *Normalised dissolution rates with respect U according to the initial inventory of the fuel fragments.*

The normalised dissolution rates plotted in Figure 23 indicate that, in spite of the scatter of the data, many of the radionuclides behave congruently with U. Furthermore, there is a clear trend of decreasing normalised dissolution rates with the time the fuel specimens have been exposed to the test solutions. After some 100 days, this is approximately 4 runs, the normalised release rates reach a steady state value around $3\ 10^{-8}$ mole/day.

Surprisingly enough, elements like Mo and Cs appear to behave congruently after an initially higher release when the fuel specimens are fresh. This differentiated behaviour could be the result of the preferential location of these radionuclides at grain boundaries /Forsyth and Werme, 1991; Forsyth, 1995/.

Np is also released congruently with U, once the initial higher dissolution of the oxidised layer of U is completed. Sr and Tc follow the matrix behaviour quite remarkably. In the next section we will perform some thermodynamic analysis of the data.

4.4.2 Thermodynamic analysis

The same equilibrium modelling approximation as the one previously reported in /Bruno et al, 1999/ has been used in order to determine to what extent the released radionuclides are solubility limited with respect to the primary source, the UO_2 spent fuel matrix, or some secondary phase formation. In order to do so, in addition to the co-dissolution analysis, the saturation indexes (defined in /Bruno et al, 1999/) of the most favoured pure solid phases have been calculated by using the analytical data from the various experiments.

Some of the elements involved undergo redox transitions and consequently the redox state of the solution has to be established in the calculations. For this purpose, the calculated pe obtained from the UO_2/U(VI) equilibrium are considered for each experiment according to the previous statements. The results are discussed element by element in the following sections.

4.4.2.1 Uranium

As we have already pointed out, the concentration of uranium in solution under the experimental conditions is limited by the extent of oxidative dissolution of the spent fuel matrix.

4.4.2.2 Plutonium

As we have already noticed in the previous analysis of results the observed plutonium concentrations in solution suggest that additional processes to matrix dissolution govern its overall behaviour.

In the first experiment 7.40.1, uranium and plutonium have similar dissolution behaviour (Figure 24). However, the Pu to U ratio calculated in this run from the experimental concentrations (see the slope of the linear regression in the plot) is lower than the one given by the inventory, $Pu/U=8.61\cdot10^{-3}$. The larger release of Pu in the first tests with respect to the subsequent ones might be attributed to the larger uranium dissolution of the oxidised surface layer provoking a larger release of the radionuclides embedded in the matrix. In addition, this larger release might be also attributed to the accessibility of the Pu located near the surface given the gradient in the radial distribution concentration of this radionuclide. This gradient can be almost a factor of 3 higher near the surface than in the centre of the pellet for LWR spent fuels of moderate burn up /Hanson, 1998/.

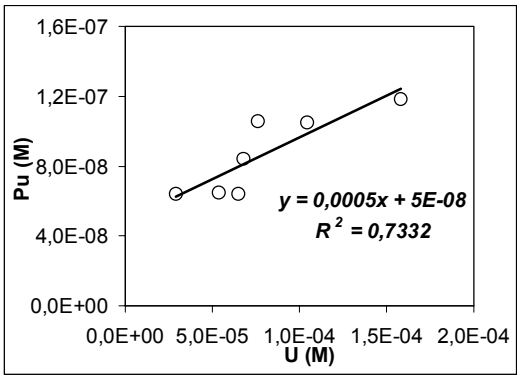

Figure 24. *Plutonium versus uranium concentrations in the first run, 7.40.1.*

According to the previous modelling carried out in /Bruno et al, 1999/ for the series 7.40.1 to 7.40.4 and the previous work of /Bruno et al, 1998/ for long term spent fuel leaching experiments, the short term behaviour of Pu from spent fuel leaching appears to be initially controlled by the formation of a $Pu(OH)_4$ poorly ordered phase.

Furthermore, once the oxidised surface layer of the fresh sample is depleted, Pu concentrations in solution reach a steady state at very short contact times. This is a clear indication of the precipitation of a secondary phase controlling the Pu concentrations in solution. Under these experimental conditions, Pu is present mainly as Pu(IV), hence solid phases of this oxidation state are considered. Consequently, the relative stability of these phases in the present experimental conditions has been explored by calculating their saturation indexes as presented in Figure 25.

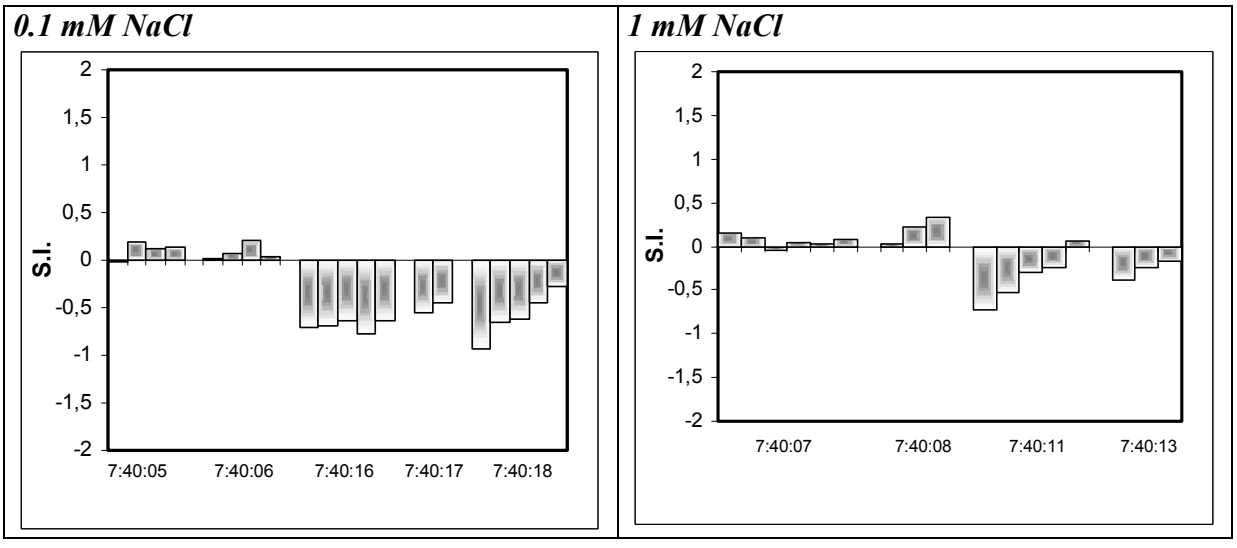

Figure 25. *Saturation indexes of $Pu(OH)_4(am)$ for series with 0.1 mM and 1 mM NaCl.*

Saturation indexes indicate that Pu concentrations in solution are close to equilibrium with $Pu(OH)_4(am)$ in most of the runs. In some of the tests, Pu concentrations in the first experimental points are undersaturated with respect to this solid, however, as the dissolution test proceeds, Pu concentrations approach saturation. This trend is a clear indication that this solid phase is controlling the release of this radionuclide under these experimental conditions. Figure 25 shows the results for series carried out with 0.1 and 1 mM of NaCl in the initial solution composition, however, this behaviour is reproducible in the other series carried out with a larger initial chloride content and without it /Bruno et al, 1999/.

4.4.2.3 Neptunium

The analysis of the primary data indicates that neptunium follows the same trend as uranium in most of the tests. Figure 26 shows the good agreement between neptunium and uranium concentrations indicating a co-dissolution of the minor radionuclide with respect to the matrix. The slope obtained from the linear regression accounts for the Np/U ratio. This ratio is very close to the one calculated based on the inventory of the fuel sample, that is Np/U = $(5.6 \pm 0.9)\cdot 10^{-4}$, indicating a congruent release of this radionuclide according to the inventory of the sample. The exception are the firsts tests (7.40.1 to 7.40.3) corresponding to the dissolution of the altered surface layer of the sample, observing a non congruent release of this radionuclide with respect the major component of the matrix and a minor release with respect to the inventory ratio.

As previously reported the initial chloride content does not have any effect on the neptunium release given that changes in solution composition among series does not affect neptunium speciation, with Np(IV) as the predominant oxidation state in the aqueous phase.

Saturation indexes are calculated considering $Np(OH)_4(s)$, the solid phase able to precipitate. As discussed in the previous report /Bruno et al, 1999/, neptunium concentrations in solution are always under saturated with respect this solid phase although the general trend is that they approach to equilibrium as the dissolution reaction proceeds. This solubility control has been also proposed in previous experimental studies /Forsyth and Werme, 1992; Forsyth, 1997/.

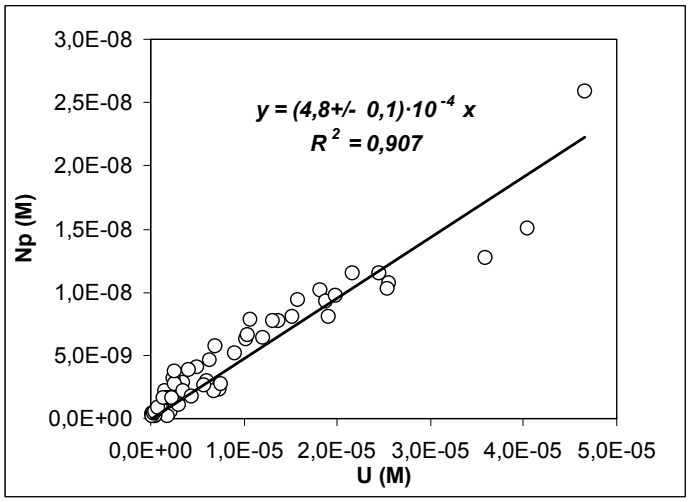

Figure 26. *Neptunium versus uranium concentrations in all the experimental series.*

The lack of equilibrium with respect any solid phase in the present experiments is expected according to the congruent dissolution mechanism considered for modelling these data along all the experimental time (Figure 11).

4.4.2.4 Strontium

According to the previous analysis of the data (Figure 12), the release of strontium in most of the tests should be controlled by the release of the fuel matrix. However, as we have previously stated, when looking at strontium data in function of time, we may observe that strontium concentrations in some of the tests seem to reach a steady-state. This trend led us to suspect that additional mechanisms to the initial release given by the matrix dissolution should occur in some of these systems. In order to support all these hypothesis we have first of all assumed that strontium dissolves congruently with the matrix, uranium, given that this radionuclide is mainly located within the matrix dissolved as oxide /Kleykamp, 1988/. Figure 27 is a plot of the Sr-90 in front of the uranium concentrations measured at the different time intervals in all those tests where strontium concentrations did not reach any steady-state and a continuous increase of strontium concentrations was observed with time.

The slope obtained from the linear regression accounting for the Sr-90 to U ratio calculated by means of solution data is quite close to the inventory ratio, having a value of Sr-90/U = $(1.51 \pm 0.17)\cdot 10^{-3}$. The independent term of the linear regression should account for the instant strontium release attributed to the enrichment of this radionuclide in the grain boundaries and gaps on the surface of the fuel /Johnson and Tait, 1997/. The agreement between the ratio calculated from solution data and the one given by the inventory of the fuel fragments is consistent with the congruent release of Sr with U reported in previous works /Forsyth and Werme, 1992/.

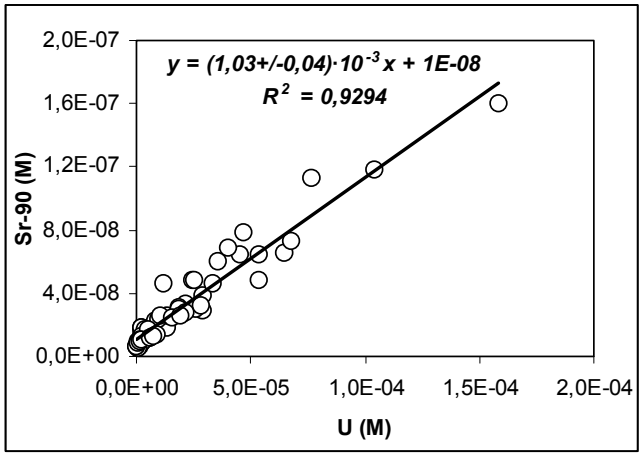

Figure 27. *Strontium versus uranium concentrations in all the tests with the exception of those reaching a steady-state for Sr-90.*

Nevertheless, as we have previously stated, some of the tests reached steady-state concentrations for strontium at relatively short contact times (Figure 12). In order to ascertain if there is some solubility control in these tests, saturation indexes have been calculated accounting for the solid phases able to precipitate under these experimental conditions, some of the results are depicted in Figure 28.

Strontianite is thermodynamically the most favourable solid phase for Sr in the experimental conditions. However, as shown in the previous figure, all solutions are clearly undersaturated with respect to this phase. Hence, the release of this element in solution is not merely controlled by its individual solubility.

The different behaviour between series was not expected given that the different solution compositions do not have to affect the solution behaviour of this element.

The behaviour of this radionuclide in these series gives an indication that its release from the fuel matrix may be controlled by the dissolution of the major component based on a congruent co-dissolution process. Nevertheless, some of the data also indicates that other mechanisms should control its concentration in solution at not very long contact times. Unfortunately, these mechanisms are difficult to ascertain with the present data available, suspecting that some sorption process or precipitation of mixed solid phases should take place.

However, the present modelling gives some different views and insights on the use of strontium as dissolution marker of the spent fuel as it has been previously stated in former works /Forsyth, 1997; Bruno et al, 1998/

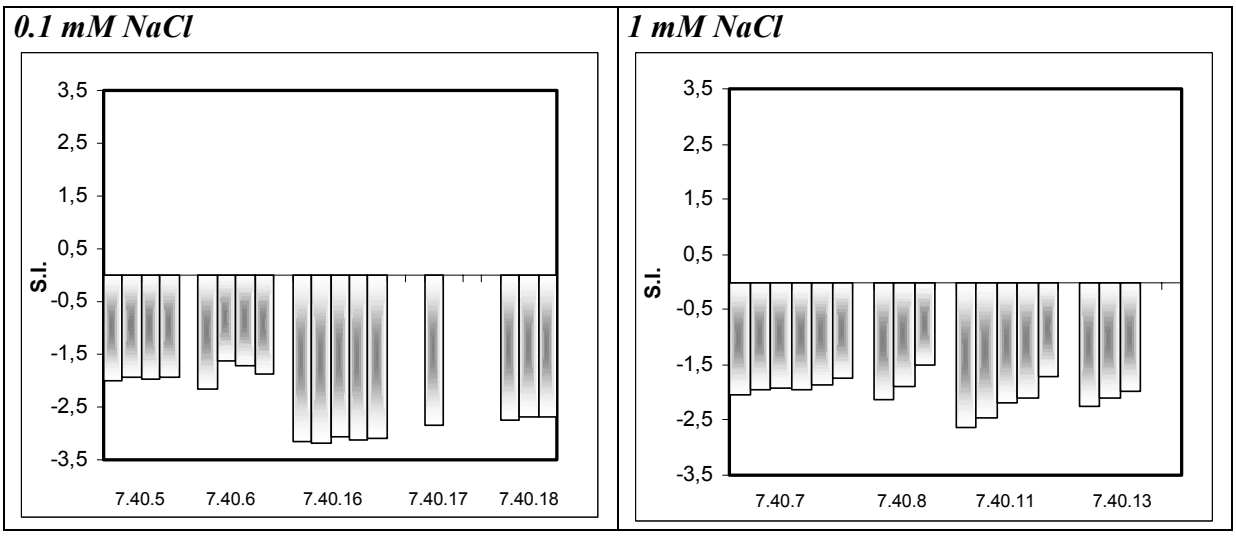

Figure 28. *Saturation indexes of strontianite ($SrCO_3(s)$) for series with 0.1 mM and 1 mM NaCl.*

4.4.2.5 Caesium

Caesium is a very soluble radionuclide and it is not solubility limited under the experimental conditions of the present tests. Therefore, the concentration in solution of this radionuclide will be limited by the dissolution of the matrix and its location within this matrix.

Two different trends with different slopes from the linear fitting are obtained from caesium data in solution. The first runs (initial tests in Figure 29) correspond to a non-congruent release of this radionuclide with respect to the fuel matrix, with a larger release of caesium than uranium. The non-congruent behaviour may be a result of the location of this radionuclide in the phase boundaries, due to its migration to the fuel/clad gaps during irradiation in the reactor /Forsyth and Werme, 1991/. According to /Forsyth, 1995/, both Cs and I show a release behaviour similar to the inert gases, Kr and Xe. Hence, fission gas release models can be applied to estimate the magnitude of the effect. /Forsyth and Werme, 1991/ determined also a rapid release during the first few weeks of long term spent fuel dissolution experiments.

The non-congruent release of caesium in the firsts leaching tests has been quantified, obtaining that 0.7% of the total caesium contained in the fuel sample is instantaneously released. This percentage is clearly lower than the ones considered in performance assessment exercises /Johnson et al, 1994; SR 97, 1999; Vieno and Nordman, 1999/.

After this initial release, caesium release fits very well when considering a co-dissolution process with the matrix, although a slightly lower Cs/U ratio than the one expected according to congruency based on the inventory ratio is obtained (subsequent runs in Figure 29). The inventory ratio for this element is $(6.21 \pm 0.81)\cdot 10^{-3}$. /Forsyth and Werme, 1991/ also observed a decrease in the release rate of this radionuclide after the instant release, until they got to a steady level. This is all consistent with our present observations.

The initial caesium concentration considered to fit the data values should reflect the enrichment of this radionuclide at the fuel surface given by its migration during irradiation and consequently a very fast initial release of this radionuclide.

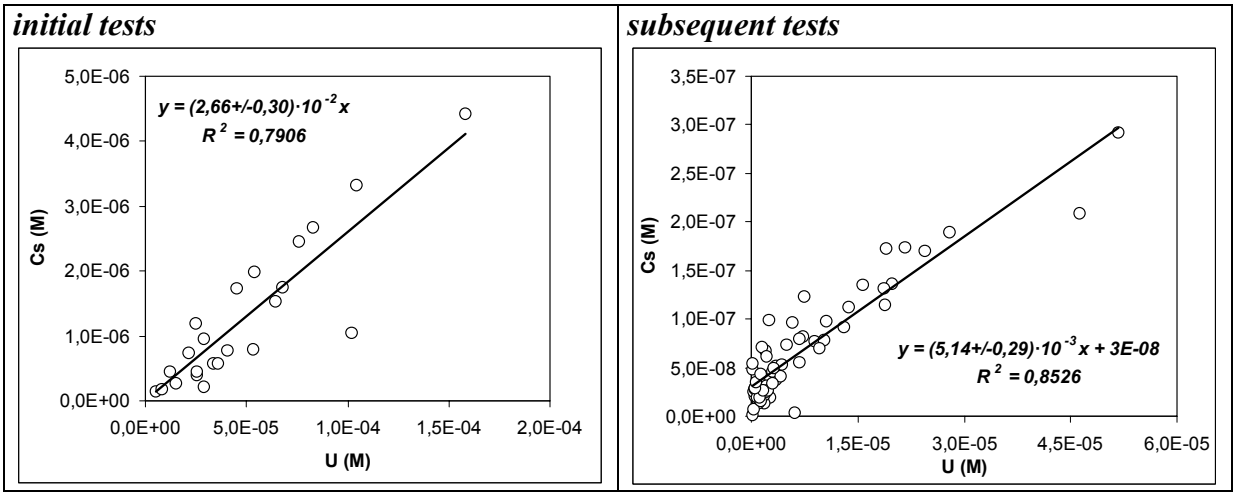

Figure 29. *Caesium versus uranium concentrations in the different experimental series.*

4.4.2.6 Molybdenum and technetium

As expected, Mo is not solubility limited under the experimental conditions of the present experiments. This is mainly due to the formation of MoO_4^- in the aqueous phase as a result of the presence of oxidants at the spent fuel/water interface, therefore, a release given by the oxidative dissolution of the molybdenum contained in the fuel is expected. On the other hand, based on the previous redox modelling performed, technetium concentrations in the aqueous phase are governed by the oxidative dissolution of metallic particles located in the fuel matrix and it is not contemplated the precipitation of any secondary solid phase. The continuous increase of technetium concentrations with time without reaching any steady state (Figure 15) lead us to disesteem the subsequent precipitation of a secondary solid phase, i.e. technetium oxide, although this process should be possible from a thermodynamic point of view. Therefore, the release of both radionuclides will be controlled by their dissolution from the fuel.

According to the previous analysis of the data, the release of these elements is close to congruency with uranium according to the inventory ratio in most of the tests. This is an unexpected result taking into account the location within the fuel matrix of these radionuclides. Mo can be found in the spent fuel forming metallic particles and also forming oxide precipitates /Kleykamp, 1988; Forsyth, 1995; Hanson, 1998/. Tc is usually forming metallic inclusions. These radionuclides have also been identified as micron size particles at or between the fuel grain boundaries and at fission gas bubbles /Forsyth, 1997/. Therefore, their release could be controlled by different processes to the matrix dissolution.

In order to study the congruent release of Mo and Tc with the matrix, Figure 30 gives two plots showing the dependence of molybdenum and technetium concentrations respectively with uranium concentrations in solution.

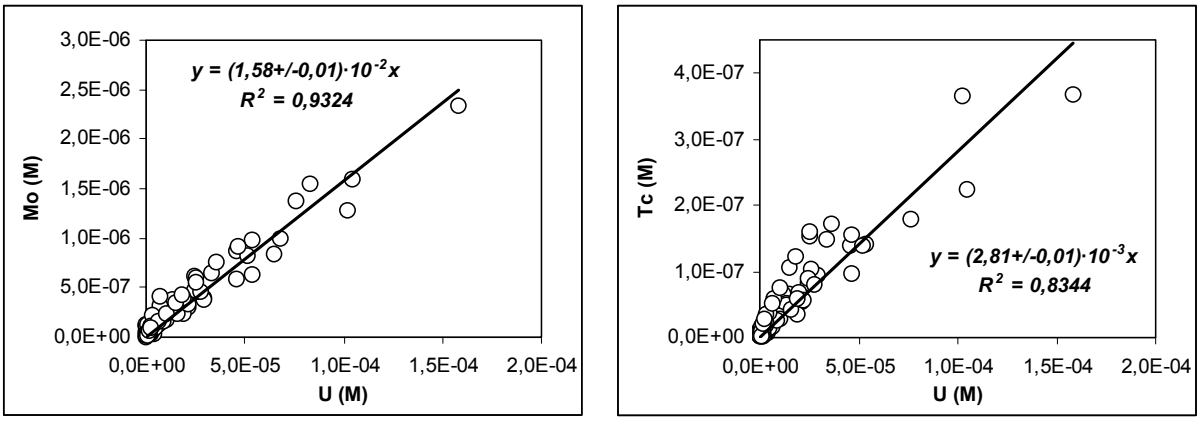

Figure 30. *Molybdenum (left) and technetium (right) versus uranium concentrations in the different experimental series.*

The linear correlation obtained in both cases corroborates a co-dissolution process of these elements with the matrix, with a good agreement between the observed ratios in solution and the inventory ratios (Mo/U = $(1.02\pm0.17)\cdot10^{-2}$ and Tc/U = $(2.49\pm0.37)\cdot10^{-3}$). A larger scatter of values is obtained for technetium data given by the lower correlation factor obtained. Nevertheless, the Tc/U calculated ratio from solution data agrees with the inventory ratio within the associated uncertainty, while Mo/U solution ratio is slightly higher to the one given by the fuel inventory. This slight difference indicates that larger molybdenum release than the one expected assuming congruency and according to the inventory ratio of the matrix occurs.

The unexpected congruent release of these radionuclides has been also reported in previous works. /Gray, 1998/ performed various flow-through tests using fuel samples with different degrees of oxidation. Tc results from these experiments were quite surprising. In some tests he observed that Tc dissolved slower than the matrix, while in other tests he obtained that Tc dissolved nearly congruently with the matrix from both oxidised and non-oxidised fuel samples. The author relates this behaviour to the location of this fission product as metallic inclusions. However, the distribution of these inclusions in the fuel seems to depend on temperature and burnup /Kleykamp, 1988/. Consequently, the variation in the Tc distribution may contribute to the variation in the Tc dissolution mechanisms.

Based on the results obtained in the drip tests under oxidising conditions within the Yucca Mountain programme, /Stout and Leider, 1998/ suggest the use of Tc as a marker element for matrix dissolution owing to its high solubility and general tendency not to become incorporated into alteration phases.

/Bruno et al, 1992/ and /Ollila, 1992/ report a congruent dissolution of Mo with the SIMFUEL matrix, after a high initial fraction release. The authors argue that according to the characterisations made to the SIMFUEL pellets, Mo is present in segregated particles located on the grain boundaries or grain edges with an appearance similar to the metallic fission product particles found in irradiated oxide fuel.

/Bruno et al, 1998/ reported the results of Tc dissolution data obtained from spent fuel leaching experiments for long contact times. Their modelling showed that only at short contact times, technetium is released congruently with uranium, in agreement with the present modelling work, the short contact times of these experiments agree with all the time interval of the present tests. However, at longer contact times, a larger release of technetium with respect to uranium occurred. This de-coupling indicated that different processes appear to control its release from the matrix, at least, at long contact times.

In addition, other works based on the results obtained from long time spent fuel leaching experiments state a technetium and molybdenum release probably controlled only by oxidation of metallic inclusions /Forsyth and Werme, 1992; Forsyth, 1997/.

In order to study to which extent the behaviour of these two redox sensitive elements is related we have studied the potential correlation in the dissolution behaviour of both radionuclides. For this purpose, we have plotted technetium concentrations in front of molybdenum concentrations to ascertain their correlation. The results are given in Figure 31.

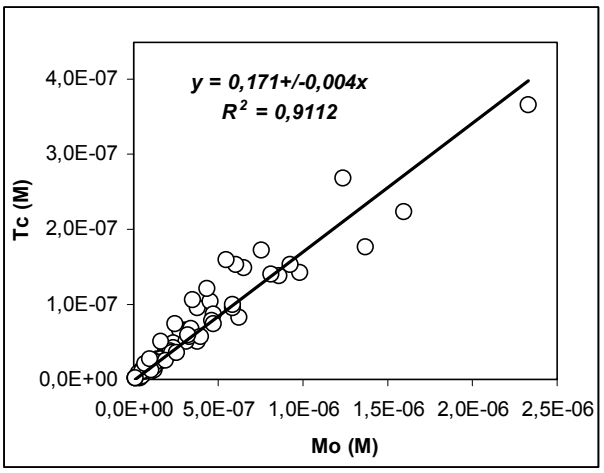

Figure 31. *Technetium versus molybdenum concentrations determined in the leaching solutions.*

The linear fitting obtained in Figure 31 indicates a good correlation between both radionuclides obtaining a ratio quite close to the one expected from the inventory ratio, 0.244±0.049. The slightly lower ratio obtained from solution data with respect to the one reported based on the fuel inventory leads to a lower technetium release than the one expected. One possible explanation should be that molybdenum has the highest affinity for oxygen and consequently it oxidises first in the metallic inclusions /Kleykamp, 1988/. This greater oxidation and consequently larger release should explain this slight difference in the ratios. The oxidation of the fuel and of the exposed metallic particles during air storage before starting each new test should also influence larger oxidation and dissolution of Mo. This is in agreement with the results obtained by Cui and co-workers /Cui et al, 2001/ on the leaching of synthesised metal aggregates in spent fuel. They observed a selective release of Mo under both reducing and air saturated conditions in Mo-Ru-Pd-Rh alloys. /Cui et al, 2001/ explained the preferential release of Mo by a metal oxidation process. Given that this metal has the lower oxidation potential with respect the other ones (Eh = –0.59 V vs. SHE), it has the larger free energy of activation and consequently it releases faster. These results are also in agreement with previous observations by /Forsyth, 1997/, who also attributes the initial major release rate obtained in his experiments to this previous oxidation due to air storage of the fuel specimens.

Hence, according to the previous discussions the experimental observations give some indications that Mo and Tc co-dissolve as the metallic particles become oxidised. These radionuclides are also released as the fuel matrix is oxidised, at least, at short contact times corresponding to the time intervals studied in the present experiments.

4.4.2.7 Yttrium and neodymium

The primary analysis of the data (Figure 16 and Figure 17) shows that the mechanisms controlling the release of these elements are not solely related to matrix dissolution. The steady state concentrations reached in most of the tests indicate that other mechanisms are controlling the release of these radionuclides from the fuel.

These results are somewhat unexpected as it is assumed that these elements have the same distribution in the fuel matrix /Forsyth, 1997/ and they are homogeneously dissolved with uranium as oxides /Kleykamp, 1988/. Therefore, at the short contact times of the present experiments, a congruent dissolution with the matrix could be expected. The incongruent release with respect to the matrix showed in Figure 32 may be explained by the fact that probably the distribution of these radionuclides in the matrix is not as homogeneous as expected. The preferential release of U with respect to these radionuclides should indicate an impoverishment of these elements in the most superficial areas of the samples.

The solutions are in general under saturated with respect to any Y and Nd pure solid phases in the present experiments. As we reported in the previous work /Bruno et al, 1999/, neodymium is close to equilibrium with $NdOHCO_3(s)$ in the first run but clearly under saturated in the subsequent ones, as we can see in Figure 33. The same applies for yttrium.

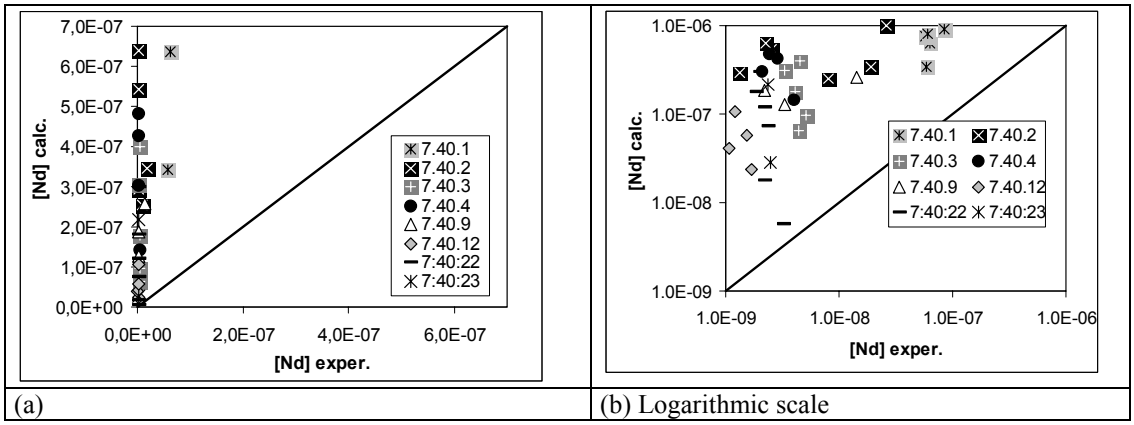

(a) (b) Logarithmic scale

Figure 32. *Calculated neodymium concentrations versus the experimental ones assuming a congruent co-dissolution process with uranium. Series without NaCl in solution.*

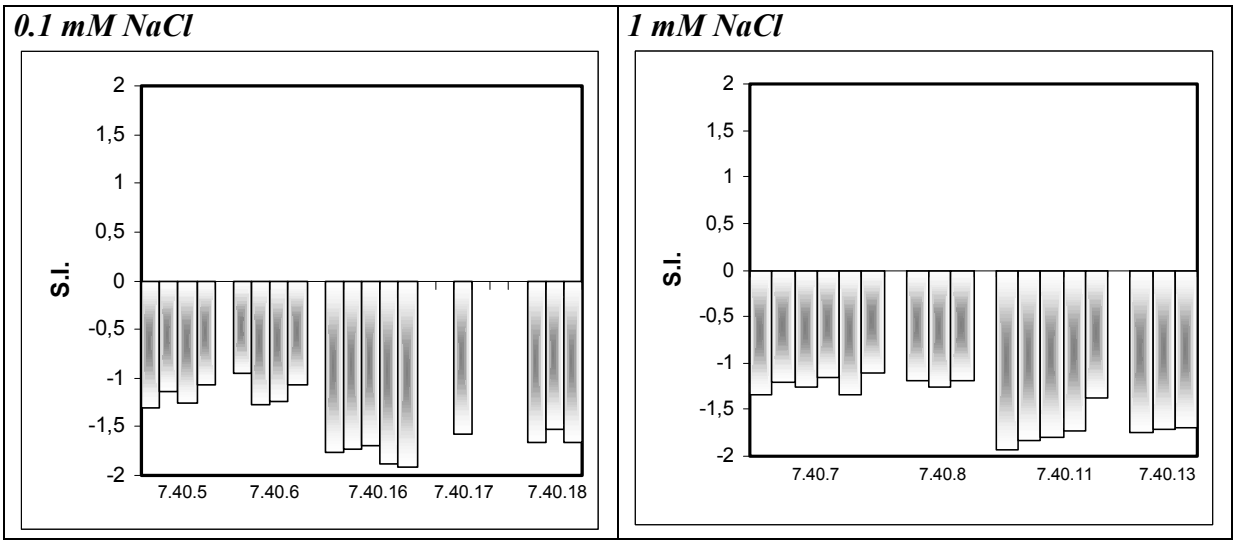

Figure 33. *Saturation indexes of $NdOHCO_3(s)$ in series with 0.1 mM and 1 mM NaCl.*

Given the present data, no conclusions can be drawn about the processes controlling the release of these elements from the fuel. /Forsyth, 1997/ suggests that lanthanide and actinide elements could be co-precipitated with or scavenged by uranium deposited, in such case, these radionuclides would be enriched in the deposit with respect the uranium. As it has been previously shown, the release of uranium in these experiments is only controlled by the oxidative dissolution of the matrix and no secondary uranium phase is formed in these experiments. Hence, such a co-precipitation process is clearly not working under the present circumstances.

Due to the chemical similarity between both radionuclides, we have studied their potential correlation in the dissolution behaviour of both elements. For this purpose, we have plotted yttrium in front of neodymium concentrations in solution (Figure 34) in order to elucidate its potential congruency in the dissolution mechanism.

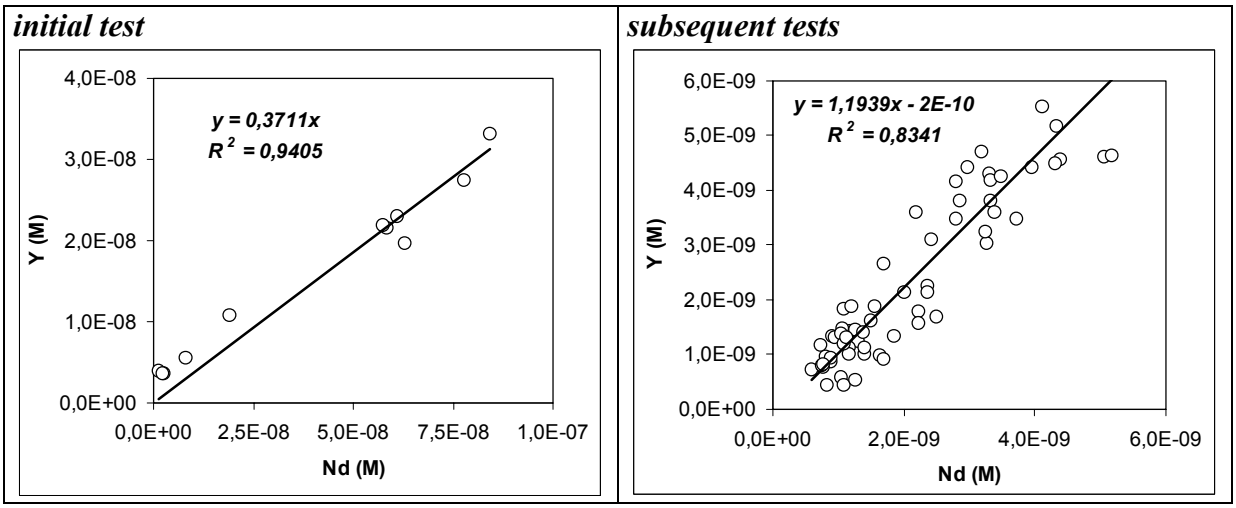

Figure 34. *Yttrium versus neodymium concentrations in solution in all the tests.*

The calculated ratio in the first two tests is quite different to the one obtained for the rest of the tests. While in the firsts tests the Y/Nd ratio is around 0.4, in the other ones this ratio approaches 1. This implies that in tests corresponding to the initial leaching of the fresh fuel surface, a preferential release of Nd with respect to Y occurred, while in the subsequent leachings their release was the same. These Y/Nd ratios do not approach the one calculated based on the inventory of the sample with a value of 0.13±0.01.

The larger calculated ratios from solution data than the inventory ratio indicates a preferential release of Y with respect to Nd. This preferential release is something surprising given the similar chemical state and homogeneous location of both radionuclides in the fuel matrix according to the reported literature /Kleykamp, 1988; Forsyth, 1997/. However, it might be related to the ionic radii, Y^{3+} = 0.88Å and Nd^{3+} = 0.995 Å /Cotton and Wilkinson, 1998/ and to their tendency to hydrolyse with the decrease of this parameter. In addition, carbonate complexation will be also stronger for Y.

At this stage, there is not sufficient data to elucidate the mechanisms controlling the release of these radionuclides from the fuel.

5 Conclusions

The present work indicates that carefully controlled mass balance radiolytic experiments are useful to ascertain the mechanisms responsible for spent fuel stability and radionuclide release under repository conditions. In this context, the time-resolved experiments have proven to be particularly suitable to gain a mechanistic insight on the key processes related to water radiolysis, matrix oxidation and radionuclide dissolution.

Concerning the production and fate of radiolytic products at the spent fuel/water interface, the present experimental data and the electron mass balance calculations analysis indicate that the excess of oxidants produced is readily scavenged by the reducing capacity of the uranium(IV) dioxide fuel matrix. The main oxidant scavenging processes are either the formation of an oxidised UO_{2+x} surface layer in deionised water, and/or the formation of soluble U(VI)-carbonate species in bicarbonate media. The formation of the oxidised surface layer has a relevant impact on the decomposition of H_2O_2 and the formation of secondary radiolytic products. The presence of chloride ions seems to have some effect on the oxidant generation by radiolytic water decomposition.

The analysis of the redox dependent components, as determined from the time-resolved experiments, indicate that a redox equilibrium situation is established between the dissolved radiolytic products (H_2, O_2 and H_2O_2), the UO_2/U(VI) and the Tc(m)/TcO_4^- redox pairs. The resulting pe in the contacting solution is around –3. This could indicate that reducing conditions are restored in the aqueous phase at sufficient distance away from the dynamic redox spent fuel/water interface. Actual redox measurements in these time-resolved experiments should be useful to validate this hypothesis.

Concerning the radionuclide dissolution data, the present experiments have helped to confirm in a more mechanistic manner some of the observations already made from the very long term spent fuel leaching experiments. Initial dissolution rates indicate the ageing effect of the fuel fragments on the release of uranium and all the radionuclides embedded in. In the overall the release rates for U and the matrix associated radionuclides are in the range of 10^{-6} (moles/day) with a clear decreasing trend with exposure time and after 2 years the initial release rates have decreased down to 3 10^{-8} moles/day.

Uranium dissolution at the early contact times is controlled by the oxidative dissolution of the UO_2 matrix. This process controls the co-dissolution of most of the measured radionuclides, Sr, Np and Pu between others. However, the solubility of the actinides appear to be limited by the formation of An(IV) hydroxide phases. This is particularly noticeable in the case of Pu. Sr-90 shows no solubility control during the whole series of experiments although a steady state is reached in some of the tests. These results give new insights in the reliability of this nuclide as matrix alteration marker. Cs behaves as expected with a preferential dissolution pattern in the first runs in agreement with previous observations, but it shows a remarkable congruent behaviour once the initial surface has been dissolved. The release of Tc and Mo appears to be controlled by the oxidative dissolution of their metallic phases, although their release seems also to be congruent with the UO_2 dissolution. The behaviour of Nd and Y is quite surprising and does not show any indication of congruent release with the fuel matrix.

Finally, no clear dependence of the radionuclide dissolution data on the initial chloride content in the leaching solutions has been observed.

6 References

Andreozzi R, Caprio V, Onsola A, Marotta R, 1999. Advanced oxidation processes (AOP) for water purification and recovery. Cat. Today, 53, 51–59.

Behar D, Czapski G, Duchovny I, 1969. Carbonate radical in flash photolysis and pulse radiolysis of aqueous carbonate solutions. J. Phys. Chem. vol 74 no 10 pp 2206–2210.

Bruno J, Casas I, Sandino A, 1992. Static and dynamic SIMFUEL dissolution studies under oxic conditions. J. Nucl. Mat., 190, 61–69.

Bruno J, Cera E, Duro L, Ahonen L, 1996. Deep groundwater redox reactions in the Palmottu uranium deposit: The role of uranium and iron in these processes. POSIVA-96-24.

Bruno J, Cera E, Duro L, Pon J, de Pablo J, Eriksen T E, 1998. Development of a kinetic model for the dissolution of the UO_2 spent nuclear fuel. Application of the model to the minor radionuclides. SKB TR-98-22. Svensk Kärnbränslehantering AB.

Bruno J, Cera E, Grivé M, 1999. Experimental determination and chemical modelling of radyolitic processes at the spent fuel/water interface. SKB TR-99-26. Svensk Kärnbränslehantering AB.

Casas I, Bruno J, 1994. What have we learned about Spent Fuel Dissolution in Cigar Lake? Within the Final Report of the AECL/SKB Cigar Lake Analog Study. SKB TR 94-04. Svensk Kärnbränslehantering AB.

Cera E, Ahonen L, Rollin C, Bruno J, Kaija J, Blomqvist R, 2002. Redox processes at the Palmottu uranium deposit. Eighth EC Natural Analogue Working Group Meeting. Proceedings of an international workshophels in Strasbourg, France from 23 to 25 March 1999. EUR 19118 EN, 183–200.

Cotton F A, Wilkinson G, 1998. Química inorgánica avanzada. Limusa Noriega Editores, 1670pp.

Cui D, Eriksen T, Eklund U-B, 2001. On metal aggregates in spent fuel, synthesis and leaching of Mo-Ru-Pd-Rh alloy. Mat. Res. Soc. Sump. Proc. vol. 663, 427–434.

Domae M, Katsumara Y, Jiang P Y, Nagaiashi R, Hasegawa C, Ishogura K, Yoshida Y, 1994. Observation of ClO_3 radical in aqueous chlorate solution by pulse radiolysis. J. Phys. Chem., 98, 190.

Eriksen T E, Ndalamba P, Christensen H, Bjergbakke E, 1989. Radiolysis of ground water: Influence of carbonate and chloride on hydrogen peroxide production. J. Radioanalytical and Nuclear Chemistry 132 (1), 19–35.

Eriksen T E, Eklund U-B, Werme L O, Bruno J, 1995. Dissolution of irradiated fuel: a radiolytic mass balance study. J. Nucl. Mater. 227, 76–82.

Ershov B G, Kelm M, Janata E, 2000. Pulse radiolysis studies of the reactions of e^-(aq) and ·OH with ClO_3^- ions in aquoeus solution. Rad. Phys. Chem., 59, 309–312.

Forsyth R S, Werme L O, 1991. Spent fuel corrosion and dissolution. SKB TR 91-60. Svensk Kärnbränslehantering AB.

Forsyth R S, Werme L O, 1992. Spent fuel corrosion and dissolution. J. Nucl. Mater. 190, 3–19.

Forsyth R, 1995. Spent nuclear fuel. A review of properties of possible relevance to corrosion processes. SKB TR-95-23. Svensk Kärnbränslehantering AB.

Forsyth R, Eklund U, 1995. Spent nuclear fuel corrosion: The application of ICP-MS to direct actinide analysis. SKB TR-95-04. Svensk Kärnbränslehantering AB.

Forsyth R, 1997. The SKB spent fuel corrosion programme. An evaluation of results from the experimental programme performed in the Studsvik hot cell laboratory. SKB TR-97-25. Svensk Kärnbränslehantering AB.

Gray W J, 1998. Spent fuel dissolution rates as a function of burnup and water chemistry. PNNL-11895.

Hanson B D, 1998. The burnup dependence of light water reactor spent fuel oxidation. PNNL-11929.

Jayson G G, Parsons B J, Swallow A J, 1973. Some simple, highly reactive, inorganic chlorine derivatives in aqueous solution. J. Chem. Soc. Far. Trans. I, 69, 1957–1607.

Johnson L H, Shoesmith D W, 1988. Spent Fuel in: Radioactive waste forms for the future (Lutze and Ewing ed), Elsevier, 635–698.

Johnson L H, LeNeveu D M, Shoesmith D W, Oscarson D W, Gray M N, Lemire R J, Garisto N C, 1994. The disposal of Canada's nuclear fuel waste: The vault model for postclosure assessment. AECL-10714.

Johnson L H, Tait J C, 1997. Release of segregated nuclides from spent fuel. SKB TR-97-18. Svensk Kärnbränslehantering AB.

Kelm M, Pashalidis I, Kim J I, 1999. Spectroscopic investigation on the formation of hypochlorite by alpha radiolysis in concentrated NaCl solutions. Appl. Rad. Isotopes, 51, 637–642.

Kelm M, Bohnert E, 2000a. Radiation chemical effects in the near-field of a final disposal site. Part I: radiolytic products formed in concentrated NaCl solutions. Nucl. Technol., 129, 118.

Kelm M, Bohnert E, 2000b. Radiation chemical effects in the near-field of a final disposal site. Part II: simulation of the radiolytic processes in concentrated NaCl solutions. Nucl. Technol., 129, 123.

Kelm M, 2001. Radiolysis products formed in chloride brines with respect to a disposal in rock salt. In: Spent Fuel Workshop 2001, September, Helsinki, Finland. Hosted by Posiva.

Kelm M, Bohnert E, 2001. Products formed from alpha radiolysis of chloride brines. Res.Chem.Intermed., vol. 27, No. 4,5, pp. 503–507.

King F, Quinn M J, Miller N H, 1999. The effect of hydrogen and gamma radiation on the oxidation of UO_2 in 0.1 mol·dm^{-3} NaCl solution. SKB TR-99-27. Svensk Kärnbränslehantering AB.

Kleykamp H, 1988. The chemical state of fission products in oxide fuels at different stages of the nuclear fuel cycle. Nucl. Techn., 80, 412–422.

Ollila K, 1992. Simfuel dissolution studies in granitic groundwater, leaching experiments at VTT. YJT 92-24.

Röllin S, Spahiu K, Eklund U-B, 2001. Determination of dissolution rates of spent fuel in carbonate solutions under different redox conditions with a flow-through experiment. J. Nuclear Materials 297(3), 231–243

Sattonnay G, Ardois C, Corbel C, Lucchini J F, Barthe M-F, Garrido F, Gosset D, 2001. Alpha-radiolysis effects on UO2 alteration in water. J. Nucl. Mater., 288, 11–19.

Shoesmith D W, 2001. Fuel corrosion processes under waste disposal conditions. J. Nucl. Mater., 282, 1–31.

SR 97, 1999. Processes in the repository evolution. Background report to SR 97. SKB TR-99-07. Svensk Kärnbränslehantering AB.

Stout R B, Leider H R, 1998. Waste Form Characteristics Report. CD-ROM Version. LLNL Report UCRL-ID-132375.

Stumm W, Morgan J J, 1981. Aquatic chemistry. John Wiley and Sons, 2nd ed.

Sunder S, Shoesmith D W, Miller N H, 1990. XPS studies of UO2 oxidation by alpha radiolysis of water at 100ºC. J. Nucl. Mater., 175, 163–169.

Sunder S, Shoesmith D W, 1991. Chemistry of uranium dioxide fuel dissolution in relation to the disposal of used nuclear fuel, Report AECL-10395, Atomic Energy of Canada Limited, 1991.

Sunder S, Shoesmith D W, Christensen H, Miller N H, 1992. Oxidation of UO_2 fuel by the products of gamma radiolysis of water. J. Nucl. Mat., 190, 78–86.

Sunder S, Christensen H, 1993. Gamma radiolysis of water solutions relevant to the nuclear fuel waste management program. Nucl. Techn., 104, 403–417.

Vieno T, Nordman H, 1999. Safety assessment of spent fuel disposal in Hästholmen, Kivetty, Olkiluoto and Romuvaara. TILA-99. Posiva 99-07.

White A F, Yee A, 1985. Aqueous oxidation-reduction kinetics associated with coupled electron-cation transfer from iron-containing silicates at 25ºC. Geochim. Cosmochim. Acta, 49, 1263–1275.

ISSN 1404-0344

CM Digitaltryck AB, Bromma, 2003